Enriched continuum for multi-scale transient diffusion coupled to mechanics

Abdullah Waseem, Thomas Heuzé, Laurent Stainier, Marc Geers, Varvara Kouznetsova

Waseem *et al. Adv. Model. and Simul. in Eng. Sci.(2020)7:14*
https://doi.org/10.1186/s40323-020-00149-2

Advanced Modeling and Simulation in Engineering Sciences

RESEARCH ARTICLE Open Access

Enriched continuum for multi-scale transient diffusion coupled to mechanics

Abdullah Waseem[1,2], Thomas Heuzé[1], Laurent Stainier[1*], Marc G. D. Geers[2] and Varvara G. Kouznetsova[2]

*Correspondence: Laurent.Stainier@ec-nantes.fr
[1]Institut de Recherche en Génie Civil et Mécanique, GeM, UMR 6183-CNRS-École Centrale de Nantes-Université de Nantes, 44321 Nantes, France
Full list of author information is available at the end of the article

Abstract

In this article, we present a computationally efficient homogenization technique for linear coupled diffusion–mechanics problems. It considers a linear chemo-mechanical material model at the fine scale, and relies on a full separation of scales between the time scales governing diffusion and mechanical phenomena, and a relaxed separation of scales for diffusion between the matrix and the inclusion. When the characteristic time scales associated with mass diffusion are large compared to those linked to the deformation, the mechanical problem can be considered to be quasi-static, and a full separation of scales can be assumed, whereas the diffusion problem remains transient. Using equivalence of the sum of virtual powers of internal and transient forces between the microscale and the macroscale, a homogenization framework is derived for the mass diffusion, while for the mechanical case, considering its quasi-static nature, the classical equivalence of the virtual work of internal forces is used instead. Model reduction is then applied at the microscale. Assuming a relaxed separation of scales for diffusion phenomena, the microscopic fields are split into steady-state and transient parts, for which distinct reduced bases are extracted, using static condensation for the steady-state part and the solution of an eigenvalue problem for the transient part. The model reduction at the microscale results in emergent macroscopic enriched field variables, evolution of which is described with a set of ordinary differential equations which are inexpensive to solve. The net result is a coupled diffusion–mechanics enriched continuum at the macroscale. Numerical examples are conducted for the cathode–electrolyte system characteristic of a lithium ion battery. The proposed reduced order homogenization method is shown to be able to capture the coupled behavior of this system, whereby high computational gains are obtained relative to a full computational homogenization method.

Keywords: Multi-scale analysis, Coupled diffusion mechanics, Model reduction, Computational homogenization

Introduction

Coupled diffusion–mechanics problems arise in many application areas, when the diffusion of solute particles causes volumetric swelling of a host material, inducing chemical stresses which in turn affect the mass flux [1,2]. It has a broad range of applications ranging from biological tissues to microelectromechanical systems devices. For example, the

swelling of brain tissues, known as edema, due to water diffusion [3] or the bending of thin plates due to chemical saturation [4]. Another typical example is the swelling of the active material due to the lithiation process in lithium-ion batteries [5], which is also governed by coupled diffusion–mechanics phenomena.

The fundamental physics behind coupled diffusion–mechanics takes place at the atomic scale where the atomic or ionic diffusion occurs [1,6]. The diffusion rate of the solute particles and the swelling of the host material depends on the atomic size of the materials involved [7] and on the activation energy which causes the jump of atoms inside the crystal lattice [8]. The jump directions and the frequencies are affected by the stresses inside the material, which in turn alter the activation energy and hence the mass flux. At the continuum level, the diffusion of species are described as driven by the gradient of the chemical potential [9]. The induced chemical stresses affect the chemical potential, which in turn influences the mass flux in the material [9–12]; this is known as the Gorsky effect [13].

This article addresses the application of coupled diffusion–mechanics described by the simulation of swelling in lithium ion batteries. A lithium ion battery consists of four components: two electrodes—a cathode and an anode, an electrolyte and the separator. Through an electro-chemical reaction, the chemical energy is converted to electrical energy in a discharge cycle; the reverse reaction takes place during the charging cycle. During charging the chemical potential across the cell forces the lithium ions to diffuse towards the anode compartment via the electrolyte while passing through the separator [14]. At the anode, the lithium ions are deposited in the active particles during an intercalation process which increases the volume of the active particle. Upon discharging, a similar reaction occurs in which the lithium in the anode is oxidized into lithium ions and electrons. The electrons flow through the external circuit to the cathode and lithium ions diffuse towards the cathode where they intercalate into the active particles.

The amount of swelling of the active particles depends on the cathode and anode materials. For example, swelling in the cathode of up to 6.5% is reported in different lithium-metal-oxides and up to 10% in lithium-cobalt-oxide [15], Silicon-based anode active particles can swell up to 300% [16]. Even when the deformation of cathode materials is small, e.g. $LiCoO_2$, $LiMn_2O_3$ and $LiFePO_4$, the cyclic lithiation and delithiation of active particles leads to cracks and loss of contact with the matrix, which gradually results in a capacity loss and eventually failure of the battery [17,18]. Hence, to design a longer lifetime and higher energy density batteries, simulation of coupled diffusion–mechanics is of primary importance [19,20].

Most of the work done in the literature on the simulation of coupled diffusion–mechanics in batteries is based on the pioneering works of Larché and Cahn [21], in which a framework for solid-state diffusion was developed for compositional changes in the solid state [5]. In general, due to its multiphysics and multiscale nature, the simulation of lithium ion batteries is a challenging task [17]. Analytical methods for the solution of coupled diffusion–mechanics problems are limited to simple geometrical shapes [22], therefore approximate solutions using numerical techniques such as finite elements are often required [17]. However, with a complex microstructures [23] and transient phenomena [24], the direct numerical simulations (DNS) become prohibitively expensive.

Computational homogenization is a well known technique to reduce the computational costs associated with the modeling of physical phenomena in complex microstructures

[25,26]. It replaces a highly heterogeneous medium with an equivalent homogeneous one by decomposing the problem into smooth macroscale and highly oscillatory microscale problems. The effective behavior is computed from a representative microscopic element (RVE) [27] and transferred to the macroscale. The computational homogenization of transient phenomena, as associated with lithium diffusion in batteries, has been the focus of research recently [24,28]. Effective responses have to be computed at each macroscopic material point at each time step, making homogenization of transient phenomena computationally demanding. For a general overview of multi-scale computational modeling of lithium ion batteries, see [29,30].

In this work, we propose a computationally efficient method for the homogenization of coupled diffusion–mechanics for the cathode material of a lithium ion battery. The homogenization of the underlying diffusion and mechanical problems is performed separately by using the method proposed in [24]. For the diffusion problem, equivalence of virtual power (extended Hill-Mandel condition) is considered, while for the mechanical problem equivalence of virtual work is used (standard Hill–Mandel). Assuming linear material properties and small strains, the relaxed separation of scales allows the decomposition of the microscopic fields into their steady-state and transient parts. The mechanical response relies on the assumption of full scale separation since the characteristic time of the elastic deformation for the considered problem is very small compared to the characteristic diffusion time [2,9]. Moreover, the characteristic diffusion time in the active material particles is several orders of magnitude larger, than the one of electrolyte (considered here as a matrix in which active particles are embedded) [28]. Therefore, the lithium ions travel instantly in the electrolyte as compared to their diffusion in the active material. This allows for a so-called relaxed separation of scales, in which diffusive species migrate instantly in the matrix and very slowly in the inclusions [31]. Next, a model reduction technique, inpired by [32] for elasto-dynamic problems and applied in [31] to heat conduction problems, can be performed to extract the reduced bases for the steady-state and transient parts of the microscopic response. Although mechanical inertia effects can be neglected, the mechanical deformation is coupled to the transient diffusion, i.e. it evolves in time with the concentration field. Hence, a decomposition of the microscopic displacement field into a steady-state and a transient part is also required.

Through model reduction, the fine scale coupled-diffusion equations are replaced by a set of ordinary differential equations for the emergent macroscopic field variables, giving rise to an enriched continuum at the macroscale. These equations are to be solved at the macroscale together with the macroscopic mass and linear momentum conservation and the constitutive effective mass flux, rate of change of concentration and stress, obtained through the reduced order homogenization. The resulting enriched continuum macroscopic problem is computationally significantly less expensive than the original fully resolved problem or the direct transient computational homogenization.

Outline

The general framework of the coupled diffusion–mechanics framework is presented in "Coupled diffusion–mechanics formulation" section, where the classical formulation in terms of concentration and strain is summarized. Next, a computationally more convenient formulation expressed in the terms of the chemical potential and strain is derived. "Computational homogenization" section presents the homogenization framework, in

which the relaxed separation of scales is defined. The downscaling is performed and the macroscopic effective constitutive responses are obtained through an upscaling procedure. The model reduction is carried out in "Model reduction leading to an enriched continuum" section. First, a finite element discretization is introduced and the partitioned equations are shown. The reduced bases are identified, the macroscopic quantities are written in terms of the coefficients of the reduced bases and finally mode selection criteria are discussed. Numerical examples for the cathode material of a lithium ion battery are presented in "Numerical examples" section.

Symbols and notation

Macroscopic quantities are represented with a bar on top: for example scalar, vector and second-order tensor macroscopic quantities are written as $\bar{a}$, $\bar{\boldsymbol{a}}$, and $\bar{\boldsymbol{A}}$, respectively. Microscopic quantities are represented without a bar; microscopic scalar, vector and second-order tensorial quantities are written as a, $\boldsymbol{a}$ and $\boldsymbol{A}$, respectively. The same Cartesian basis is adopted at the macro and micro scales. The dot products between two vectors, and between a second-order tensor and a vector are represented as $\boldsymbol{a}\cdot\boldsymbol{b} := a_i b_i$ and $\boldsymbol{A}\cdot\boldsymbol{a} := A_{ij}a_j\boldsymbol{e}_i$, respectively. A tensorial dyadic product is denoted as $\boldsymbol{a}\otimes\boldsymbol{b} := a_i b_j \boldsymbol{e}_i\otimes\boldsymbol{e}_j$ and $\boldsymbol{A}\otimes\boldsymbol{a} := A_{ij}a_k\boldsymbol{e}_i\otimes\boldsymbol{e}_j\otimes\boldsymbol{e}_k$. The gradient of a scalar and a vector is defined as $\boldsymbol{\nabla}a := \frac{\partial a}{\partial x_i}\boldsymbol{e}_i$ and $\boldsymbol{\nabla}\boldsymbol{a} := \frac{\partial a_i}{\partial x_j}\boldsymbol{e}_i\otimes\boldsymbol{e}_j$. Similarly, the divergence operates as $\boldsymbol{\nabla}\cdot\boldsymbol{a} := \frac{\partial a_i}{\partial x_i}$ and $\boldsymbol{\nabla}\cdot\boldsymbol{A} := \frac{\partial A_{ij}}{\partial x_i}\boldsymbol{e}_j$. For linear algebra operations, columns are represented with a tilde underneath a lowercase letter, e.g. $\underset{\sim}{a}$, and matrices are represented with a bar underneath an uppercase letter e.g. $\underline{A}$. The matrices and columns of vectors and tensor quantities are written with bold symbol, for example a matrix of a vector or a tensor quantity is written as $\underline{\boldsymbol{A}}$. A tensorial product between two column arrays of vectors is defined as $\underset{\sim}{\boldsymbol{a}}^T \underline{\otimes} \underset{\sim}{\boldsymbol{b}}$, where

$$\underline{\otimes} := \begin{bmatrix} \otimes & 0 & \dots & 0 \\ 0 & \otimes & & \vdots \\ \vdots & & \ddots & \\ 0 & 0 & \dots & \otimes \end{bmatrix}. \tag{1}$$

The microscopic domain and its boundary are represented by Ω and $\partial\Omega$, respectively. The volume average of a microscopic quantity $\bullet$ is defined as

$$\left\langle \bullet \right\rangle := \frac{1}{V}\int_\Omega \bullet \mathrm{d}\Omega, \tag{2}$$

where $V = \int_\Omega \mathrm{d}\Omega$ is the volume of the microscopic domain Ω.

Coupled diffusion–mechanics formulation

Coupled diffusion–mechanics equations describing the fully resolved (heterogeneous) problem are presented in this section. The conservation laws and the boundary conditions are written for the chemical and mechanical problems, followed by the derivation of the form of the constitutive equations [9]. First, the formulation considering the concentration and the displacement (strain) as the primary field variables is presented, which requires C^1-continuity and is therefore cumbersome to implement numerically. Next, using a Legendre transform, the primal field variables are transformed to the chemical potential and strain [24]. This formulation requires only C^0-continuity and standard finite elements can be used for the implementation. Finally, the material model to be used for the microscale constituents is presented.

Conservation laws

To take into account the large time scales associated with the mass diffusion problem a transient mass conservation equation is considered (without the volumetric source/sink term)

$$\nabla \cdot \boldsymbol{j} + \dot{c} = 0 \qquad \text{in } \Omega, \tag{3}$$

which states that the divergence of the mass flux $\boldsymbol{j}$ in a domain Ω[1] is opposite to the time rate of the concentration field $\dot{c}$. Equation (3) is supplemented with Dirichlet and Neumann boundary conditions, plus an initial condition

$$\begin{aligned} c &= \widehat{c} \qquad \text{on } \partial\Omega_{\widehat{c}}, \\ \boldsymbol{j} \cdot \boldsymbol{n} &= \widehat{j}_n \qquad \text{on } \partial\Omega_{\widehat{j}_n}, \\ c(0) &= c_0 \qquad \text{at } t = 0, \end{aligned} \tag{4}$$

where $\widehat{c}$ is the prescribed value of the concentration field on the Dirichlet part of the boundary $\partial\Omega_{\widehat{c}}$, and $\widehat{j}_n$ is the prescribed normal outward mass flux on the Neumann part of the boundary $\partial\Omega_{\widehat{j}_n}$ such that $\partial\Omega_{\widehat{c}} \cup \partial\Omega_{\widehat{j}_n} = \partial\Omega$ and $\partial\Omega_{\widehat{c}} \cap \partial\Omega_{\widehat{j}_n} = \varnothing$. The initial value of the concentration at time $t = 0$ is denoted by c_0.

Considering the short characteristic times of phenomena associated with the mechanical problem, it is justified to assume a conservation of linear momentum neglecting inertial terms, which without volumetric forces reads

$$\nabla \cdot \boldsymbol{\sigma} = \boldsymbol{0} \qquad \text{in } \Omega, \tag{5}$$

requiring the divergence of stress field $\boldsymbol{\sigma}$ in a body Ω vanish. Conservation of linear momentum (5) is also supplemented with the Dirichlet and Neumann boundary conditions

$$\begin{aligned} \boldsymbol{u} &= \widehat{\boldsymbol{u}} \qquad \text{on } \partial\Omega_{\widehat{\boldsymbol{u}}}, \\ \boldsymbol{\sigma} \cdot \boldsymbol{n} &= \boldsymbol{t}_n \qquad \text{on } \partial\Omega_{\widehat{\boldsymbol{t}}_n}, \end{aligned} \tag{6}$$

where $\boldsymbol{u}$ is the displacement field, $\widehat{\boldsymbol{u}}$ is the prescribed displacement value on the Dirichlet part of the boundary $\partial\Omega_{\widehat{\boldsymbol{u}}}$, and $\widehat{\boldsymbol{t}}_n$ is the traction force applied on the Neumann part of the boundary $\partial\Omega_{\boldsymbol{t}_n}$ such that $\partial\Omega_{\widehat{\boldsymbol{u}}} \cup \partial\Omega_{\boldsymbol{t}_n} = \partial\Omega$ and $\partial\Omega_{\widehat{\boldsymbol{u}}} \cap \partial\Omega_{\boldsymbol{t}_n} = \varnothing$. Constitutive equations for the mass flux $\boldsymbol{j}$, the concentration c and the stress $\boldsymbol{\sigma}$ are required to close the problem (3)–(6).

(c, $\boldsymbol{\varepsilon}$) formulation

Following [9], the dissipation inequality for a coupled diffusion–mechanics problem can be written as

$$\varphi = \boldsymbol{\sigma} : \dot{\boldsymbol{\varepsilon}} + \mu\dot{c} - \dot{\psi} - \boldsymbol{j} \cdot \nabla\mu \geq 0, \tag{7}$$

where μ is the chemical potential, φ is the dissipation density at a material point $\boldsymbol{x}$ and $\dot{\psi}$ is the time derivative of the Helmholtz's free energy density. For coupled diffusion–mechanics problems, the Helmholtz's free energy density ψ depends on the concentration field c and the strain $\boldsymbol{\varepsilon}$, related to the displacement field $\boldsymbol{u}$ by $\boldsymbol{\varepsilon} = \text{sym}(\nabla\boldsymbol{u})$ (assuming linear kinematics). Using the chain-rule, its material time derivative can be written as

$$\dot{\psi} = \dot{\psi}(c, \boldsymbol{\varepsilon}) = \frac{\partial\psi}{\partial c}\dot{c} + \frac{\partial\psi}{\partial\boldsymbol{\varepsilon}} : \dot{\boldsymbol{\varepsilon}}, \tag{8}$$

[1] Here, the domain Ω is used as a general description of a continuum body and should not be confused with the description of a microscopic domain in computational homogenization.

substituting the expression of $\dot{\psi}$ from Eq. (8) into the dissipation inequality (7) and rearranging terms yields

$$\varphi = \left(\boldsymbol{\sigma} - \frac{\partial \psi}{\partial \boldsymbol{\varepsilon}}\right) : \dot{\boldsymbol{\varepsilon}} + \left(\mu - \frac{\partial \psi}{\partial c}\right) \dot{c} - \boldsymbol{j} \cdot \nabla \mu \geq 0. \tag{9}$$

In the inequality (9), the restriction on the dissipation density to be positive is partially fulfilled by setting

$$\boldsymbol{\sigma} = \frac{\partial \psi}{\partial \boldsymbol{\varepsilon}} \qquad \text{and} \qquad \mu = \frac{\partial \psi}{\partial c}, \tag{10}$$

which provides, for a given expression for the Helmholtz potential ψ, the constitutive equations for the stress and the chemical potential, respectively. Considering a quadratic Helmholtz free energy density [9]

$$\psi = \psi(c, \boldsymbol{\varepsilon}) = \frac{1}{2}\boldsymbol{\varepsilon} : \mathbb{C} : \boldsymbol{\varepsilon} + \boldsymbol{S} : \boldsymbol{\varepsilon}(c - c_0) + \frac{1}{2}\Lambda(c - c_0)^2, \tag{11}$$

results in linear constitutive expressions for the stress and the chemical potential given by

$$\boldsymbol{\sigma} = \frac{\partial \psi}{\partial \boldsymbol{\varepsilon}} = \mathbb{C} : \boldsymbol{\varepsilon} + \boldsymbol{S}(c - c_0), \tag{12}$$

and

$$\mu = \frac{\partial \psi}{\partial c} = \boldsymbol{S} : \boldsymbol{\varepsilon} + \Lambda(c - c_0), \tag{13}$$

where $\mathbb{C}$ is the elastic stiffness tensor, $\boldsymbol{S}$ the chemical strain modulus tensor, c_0 the initial concentration and Λ is the chemical modulus. The constitutive model based on energy density function given in Eq. (11) is an alternative approach to the approach in which the microscopic strain field is decomposed in an elastic and volumetric swelling part, for more details see [33] . The remaining dissipation term in (9)

$$-\boldsymbol{j} \cdot \nabla \mu \geq 0, \tag{14}$$

asserts a restriction on the constitutive form of the mass flux $\boldsymbol{j}$. Here, we use Fick's second law which states that the mass flux $\boldsymbol{j}$ depends linearly on the gradient of the chemical potential $\nabla \mu$ i.e.

$$\boldsymbol{j} = -\boldsymbol{M} \cdot \nabla \mu, \tag{15}$$

where $\boldsymbol{M}$ is the second-order mobility tensor which has to be positive definite to satisfy (14). Next, the constitutive Eqs. (12), (13) and (15) can be introduced in the mass conservation Eq. (3),

$$\nabla \cdot [\boldsymbol{M} \cdot \nabla(\Lambda(c - c_0) + \boldsymbol{S} : \boldsymbol{\varepsilon})] - \dot{c} = 0, \tag{16}$$

and in the conservation of linear momentum (5)

$$\nabla \cdot [\mathbb{C} : \boldsymbol{\varepsilon} + \boldsymbol{S}(c - c_0)] = \boldsymbol{0}. \tag{17}$$

The mass and the linear momentum conservation Eqs. (16) and (17) can be solved together for the concentration and displacement fields $(c, \boldsymbol{u})$. Equation (16), however, involves the third-order derivative of $\boldsymbol{u}$ and its numerical solution therefore requires a C^1-continuous finite element formulation. Various other solution techniques have also been proposed in the literature for this type of problems, see for example [24,34]. In the current work, following [24], a Legendre transform is performed on the Helmholtz's free energy density function $\psi(c, \boldsymbol{\varepsilon})$ to obtain a dual energy density function ω, for which the primary field variables are the chemical potential μ and the strain $\boldsymbol{\varepsilon}$.

(μ, $\boldsymbol{\varepsilon}$) formulation

Now, we derive the constitutive equations for stress $\boldsymbol{\sigma}$, concentration c and mass flux $\boldsymbol{j}$ considering (μ, $\boldsymbol{\varepsilon}$) as the primary field variables. A Legendre transform can be performed on the Helmholtz's free energy density function (11) to obtain the dual energy density function ω

$$\omega(\mu, \boldsymbol{\varepsilon}) = \psi(c(\mu, \boldsymbol{\varepsilon}), \boldsymbol{\varepsilon}) - \mu c(\mu, \boldsymbol{\varepsilon}), \tag{18}$$

which is now a function of the chemical potential μ and the strain $\boldsymbol{\varepsilon}$. The constitutive equations for the concentration and the stress fields (c, $\boldsymbol{\sigma}$) can be obtained by the standard Coleman–Noll procedure. Substituting $\psi = \omega + \mu c$ from (18) into (7) provides the dissipation inequality

$$\varphi = \boldsymbol{\sigma} : \dot{\boldsymbol{\varepsilon}} - \dot{\omega} - \dot{\mu} c - \boldsymbol{j} \cdot \boldsymbol{\nabla} \mu \geq 0. \tag{19}$$

Using the chain-rule, the time derivative of the dual energy density $\dot{\omega}$ can be written as

$$\dot{\omega}(\mu, \boldsymbol{\varepsilon}) = \frac{\partial \omega}{\partial \mu} \dot{\mu} + \frac{\partial \omega}{\partial \boldsymbol{\varepsilon}} : \dot{\boldsymbol{\varepsilon}}. \tag{20}$$

Substituting the expression for $\dot{\omega}$, from Eq. (20), into the dissipation inequality (19) and rearranging terms yields

$$\varphi = \left(\boldsymbol{\sigma} - \frac{\partial \omega}{\partial \boldsymbol{\varepsilon}} \right) : \dot{\boldsymbol{\varepsilon}} - \left(c + \frac{\partial \omega}{\partial \mu} \right) \dot{\mu} - \boldsymbol{j} \cdot \boldsymbol{\nabla} \mu \geq 0. \tag{21}$$

From here, the constitutive forms for the stress $\boldsymbol{\sigma}$ and the concentration field c are found as

$$\boldsymbol{\sigma} = \frac{\partial \omega}{\partial \boldsymbol{\varepsilon}} \qquad \text{and} \qquad c = -\frac{\partial \omega}{\partial \mu}. \tag{22}$$

Using constitutive Eq. (22) in conjunction with (18) and (11) provides the constitutive equations for the stress

$$\boldsymbol{\sigma} = \frac{\partial \omega}{\partial \boldsymbol{\varepsilon}} = \left(\mathbb{C} - \frac{\boldsymbol{S} \otimes \boldsymbol{S}}{\Lambda} \right) : \boldsymbol{\varepsilon} + \frac{\mu \boldsymbol{S}}{\Lambda}, \tag{23}$$

and for the concentration field

$$c = -\frac{\partial \omega}{\partial \mu} = \frac{\mu}{\Lambda} - \frac{\boldsymbol{S}}{\Lambda} : \boldsymbol{\varepsilon} + c_0. \tag{24}$$

For the remaining dissipation term $-\boldsymbol{j} \cdot \boldsymbol{\nabla} \mu \geq 0$, again Fick's second law (15) can be used. Introducing the stress (23), the concentration field (24) and the mass flux (15) into the mass conservation (3) gives

$$\boldsymbol{\nabla} \cdot (\boldsymbol{M} \cdot \boldsymbol{\nabla} \mu) + \frac{\boldsymbol{S} : \dot{\boldsymbol{\varepsilon}}}{\Lambda} - \frac{\dot{\mu}}{\Lambda} = 0, \tag{25}$$

while the conservation of linear momentum (5) reads

$$\boldsymbol{\nabla} \cdot \left[\left(\mathbb{C} - \frac{\boldsymbol{S} \otimes \boldsymbol{S}}{\Lambda} \right) : \boldsymbol{\varepsilon} + \frac{\mu \boldsymbol{S}}{\Lambda} \right] = \boldsymbol{0}, \tag{26}$$

Equations (25) and (26) are solved for the chemical potential μ and the displacement $\boldsymbol{u}$. The requirement of C^1-continuity on $\boldsymbol{u}$ is now relaxed by using the (μ, $\boldsymbol{\varepsilon}$) formulation, as can be seen from (26), for which a standard C^0-continuous finite element formulation can be used.

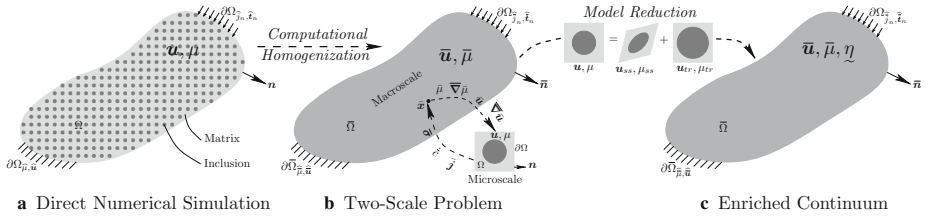

a Direct Numerical Simulation **b** Two-Scale Problem **c** Enriched Continuum

Fig. 1 Steps involved in the development of the enriched continuum formulation: first, performing computational homogenization, the solution of a highly heterogeneous problem also known as the direct numerical simulation (**a**) is replaced by a two-scale macro and microscale coupled problem (**b**), next model reduction is performed at the microscale yielding an enriched continuum formulation (**c**)

Linear isotropic constitutive model

A isotropic material model is considered for both mass diffusion and mechanical problems. The isotropic mobility tensor is given by

$$\boldsymbol{M} = M\boldsymbol{I}, \tag{27}$$

where $\boldsymbol{I}$ is the second order identity tensor and M is the scalar mobility coefficient. The chemical strain modulus $\boldsymbol{S}$ is assumed to have the following form [2]

$$\boldsymbol{S} = -\gamma K\boldsymbol{I}, \tag{28}$$

where $K = \frac{3\lambda+2G}{3}$ is the bulk modulus, λ, G are Lamé's constants and γ is the partial molar volume of the material, which is the volumetric increase of a material by the introduction of one mole of other substance. The linear elastic stiffness tensor $\mathbb{C}$ is expressed in terms of Lamé's constants as

$$\mathbb{C} = \lambda\boldsymbol{I}\otimes\boldsymbol{I} + 2G\mathbb{I}, \tag{29}$$

where $\mathbb{I}$ is the fourth order identity tensor. Next, the computational homogenization framework for the two-scale coupled diffusion–mechanics problem will be presented.

Computational homogenization

In this section, the computational homogenization of a two-scale coupled diffusion–mechanics problem is presented. First, the separation of scales regimes are defined for the mass diffusion and mechanics problems. Then, the governing equations at the micro- and the macro-scales are presented. The boundary conditions on the microscopic domain are defined through the constraints imposed by the downscaling relations. Finally, the upscaling is performed via equivalence of the virtual powers of the macro- and micro-scales providing the constitutive forms for the macroscopic quantities.

The solution of the coupled diffusion mechanics problem on the fully resolved heterogeneous domain, as shown in Fig. 1a, is referred to as direct numerical simulation (DNS). Due to the computational expense of the DNS problem it is preferred, when possible, to divide the problem into micro and macro scales and solve a homogenized problem in a two-scale manner, as shown in Fig. 1b. The homogenizability of the DNS problem depends on the separation of scales, which is discussed next.

Separation of scales

The separation of scales can be defined through the material properties of the constituents, their characteristic length and time scales, and the characteristic scales of the physical

phenomena under consideration [35]. For the coupled problem studied here, *coupled scales* for the mass diffusion, have to be considered, while for the mechanical phenomena a *full separation of scales* can be assumed. For more details on separation of scales see for example [35].

Mechanics: For the mechanical problem, a full separation of scales is adopted since the microscopic characteristic length scales ($\ell_i < \ell_m$) are much smaller than the macroscopic characteristic length scale L, which is typically the length over which the macroscopic fields vary over time i.e.

$$(\ell_i < \ell_m) \ll L, \tag{30}$$

where ℓ_m and ℓ_i are the characteristic lengths of the microstructural components (matrix and inclusions, respectively) and L.

Mass diffusion In the mass diffusion problem, the separation of scales can be quantified based on the characteristic times associated with each material constituent. The characteristic times for the matrix t_m and the inclusion t_i can be written as

$$t_m := \frac{\ell_m^2}{\mathcal{D}_m} \quad \text{and} \quad t_i := \frac{\ell_i^2}{\mathcal{D}_i}, \tag{31}$$

where $\mathcal{D}_m$ and $\mathcal{D}_i$ are the mass diffusivity coefficients of the matrix and inclusions, respectively. In the present work, a *relaxed separation of scales* is considered for the diffusion problem, which is a special case of coupled scales. In the regime of relaxed separation of scales, the characteristic diffusion time of the matrix t_m is very small compared to the one of the inclusion t_i, and the macroscopic loading time T:

$$t_m \ll (T \sim t_i). \tag{32}$$

A relaxed separation of scales is applicable to the homogenization of mass diffusion problems in lithium-ion batteries, where the lithium ions diffuse essentially instantaneously through the electrolyte material (matrix) in contrast to the very slow diffusion in the active particles (inclusions). The relaxed separation of scales has a direct implication for the model reduction presented in "Model reduction leading to an enriched continuum" section, since it allows the decomposition of the microscopic solution fields into the steady-state and transient parts. The separation of scales also indicates whether the transient terms in the conservation laws at the micro- and macro-scales should be included or not. These conservation laws are stated next.

Conservation laws at micro and macroscales

Mass conservation the mass conservation at the macroscale reads:

$$\overline{\nabla} \cdot \bar{\boldsymbol{j}} + \dot{\bar{c}} = 0 \qquad \text{in } \overline{\Omega}, \tag{33}$$

where $\bar{\boldsymbol{j}}$ and $\dot{\bar{c}}$ are the macroscopic mass flux and the macroscopic rate of change of the concentration field, respectively. To capture the time dependent mass diffusion behavior inside transient inclusions, the mass conservation is considered at the microscale:

$$\nabla \cdot \boldsymbol{j} + \dot{c} = 0 \qquad \text{in } \Omega, \tag{34}$$

where $\boldsymbol{j}$ and $\dot{c}$ are the mass flux and the rate of change of concentration at the microscale.

Conservation of linear momentum For the considered problem, mechanical inertia can be neglected, for which the macroscopic linear momentum balance equation reads:

$$\overline{\nabla} \cdot \bar{\boldsymbol{\sigma}} = \boldsymbol{0} \qquad \text{in } \overline{\Omega}, \tag{35}$$

where $\bar{\boldsymbol{\sigma}}$ is the macroscopic stress tensor. Given the full separation of scales for the mechanical problem, the conservation of linear momentum at the microscale also does not include transient terms neither and reads

$$\nabla \cdot \boldsymbol{\sigma} = \mathbf{0} \qquad \text{in } \Omega. \tag{36}$$

where $\boldsymbol{\sigma}$ is the microscopic stress tensor.

The constitutive equations for the macroscopic quantities $\bar{\sigma}$, $\bar{\boldsymbol{j}}$ and $\dot{\bar{c}}$ are yet unknown; in the computational homogenization, these are obtained through an upscaling procedure. The boundary and initial conditions at the macroscale are given by the particular problem at hand. At the microscale, the constitutive equation for $\boldsymbol{\sigma}$, $\boldsymbol{j}$ and c are assumed to be known, as presented in "Coupled diffusion–mechanics formulation" section. The boundary conditions at the microscale are obtained by downscaling relations, which will be presented next.

Downscaling

In first-order computational homogenization, the microscopic fields are approximated as the first-order Taylor's series expansion around a macroscopic point $\bar{\boldsymbol{x}}$. The chemical potential μ in a microscopic domain Ω can then be written as

$$\mu(\bar{\boldsymbol{x}}, \boldsymbol{x}, t) := \bar{\mu}(\bar{\boldsymbol{x}}, t) + \overline{\nabla}\bar{\mu}(\bar{\boldsymbol{x}}, t) \cdot [\boldsymbol{x} - \bar{\boldsymbol{x}}] + \tilde{\mu}(\bar{\boldsymbol{x}}, \boldsymbol{x}, t), \tag{37}$$

where $\bar{\mu}$ and $\overline{\nabla}\bar{\mu}$ are the macroscopic chemical potential and its gradient, respectively, and $\tilde{\mu}$ is the fluctuation field of the chemical potential at the microscale. The latter is due to the difference in material properties of the constituents, and the transient loading conditions at the macroscale. Similarly, the microscopic displacement field $\boldsymbol{u}$ can also be expressed as the first order Taylor's series expansion around a macroscopic point $\bar{\boldsymbol{x}}$

$$\boldsymbol{u}(\bar{\boldsymbol{x}}, \boldsymbol{x}, t) := \bar{\boldsymbol{u}}(\bar{\boldsymbol{x}}, t) + \overline{\nabla}\bar{\boldsymbol{u}}(\bar{\boldsymbol{x}}, t) \cdot [\boldsymbol{x} - \bar{\boldsymbol{x}}] + \tilde{\boldsymbol{u}}(\bar{\boldsymbol{x}}, \boldsymbol{x}, t), \tag{38}$$

where $\bar{\boldsymbol{u}}$ and $\overline{\nabla}\bar{\boldsymbol{u}}$ are the macroscopic displacement field and its gradient, respectively, and $\tilde{\boldsymbol{u}}$ is the microfluctuation of the displacement field.

In computational homogenization, downscaling is referred to as the transfer of macroscopic quantities to the microscale, as shown in Fig. 1b. Macroscopic quantities which are to be transferred to the microscale depend on the physical phenomena under consideration. For instance, in first-order transient computational homogenization, both for diffusion processes [36] and dynamics [37,38], both the primary macroscopic field and its gradient are transferred to the microscale. In a steady-state/static computational homogenization scheme, only the gradient information needs to be transferred to the microscale.

In transient computational homogenization, the first constraint on the microscale solution is that the volume average of the microscopic primary field is enforced to be equal to the corresponding macroscopic field

$$\begin{aligned} \left\langle \mu(\bar{\boldsymbol{x}}, \boldsymbol{x}, t) \right\rangle &= \bar{\mu}(\bar{\boldsymbol{x}}, t), \\ \left\langle \boldsymbol{u}(\bar{\boldsymbol{x}}, \boldsymbol{x}, t) \right\rangle &= \bar{\boldsymbol{u}}(\bar{\boldsymbol{x}}, t), \end{aligned} \tag{39}$$

which, by using the definitions (37) and (38) a chosen positioning of the microscopic domain such that $\langle \boldsymbol{x} - \bar{\boldsymbol{x}} \rangle = \mathbf{0}$, requires that the average of the microfluctuations over the microscopic domain vanishes

$$\begin{aligned} \left\langle \tilde{\mu}(\bar{\boldsymbol{x}}, \boldsymbol{x}, t) \right\rangle &= 0, \\ \left\langle \tilde{\boldsymbol{u}}(\bar{\boldsymbol{x}}, \boldsymbol{x}, t) \right\rangle &= \mathbf{0}. \end{aligned} \tag{40}$$

The second constraint on the microscopic solution fields is that the average of the microscopic gradient fields should be equal to the corresponding macroscopic gradients

$$\begin{aligned}\Big\langle \nabla \mu(\tilde{\boldsymbol{x}}, \boldsymbol{x}, t)\Big\rangle &= \overline{\nabla}\bar{\mu}(\bar{\boldsymbol{x}}, t),\\ \Big\langle \nabla \boldsymbol{u}(\tilde{\boldsymbol{x}}, \boldsymbol{x}, t)\Big\rangle &= \overline{\nabla}\bar{\boldsymbol{u}}(\bar{\boldsymbol{x}}, t),\end{aligned} \tag{41}$$

which by using Eqs. (37) and (38) and the identity $\nabla(\boldsymbol{x} - \bar{\boldsymbol{x}}) = \boldsymbol{I}$ can be written as

$$\begin{aligned}\Big\langle \nabla \mu(\tilde{\boldsymbol{x}}, \boldsymbol{x}, t)\Big\rangle &= \overline{\nabla}\bar{\mu}(\bar{\boldsymbol{x}}, t) + \Big\langle \nabla \tilde{\mu}(\tilde{\boldsymbol{x}}, \boldsymbol{x}, t)\Big\rangle,\\ \Big\langle \nabla \boldsymbol{u}(\tilde{\boldsymbol{x}}, \boldsymbol{x}, t)\Big\rangle &= \overline{\nabla}\bar{\boldsymbol{u}}(\bar{\boldsymbol{x}}, t) + \Big\langle \nabla \tilde{\boldsymbol{u}}(\tilde{\boldsymbol{x}}, \boldsymbol{x}, t)\Big\rangle.\end{aligned} \tag{42}$$

The last terms in the above equations, i.e. the average of the gradient of the microfluctuation fields $\langle \nabla \tilde{\mu} \rangle$ and $\langle \nabla \tilde{\boldsymbol{u}} \rangle$ should vanish to satisfy the requirements (41). After applying Gauss's theorem, these can be written as

$$\begin{aligned}\int_{\partial\Omega} \tilde{\mu}\boldsymbol{n}\mathrm{d}\Gamma &= \boldsymbol{0},\\ \int_{\partial\Omega} \tilde{\boldsymbol{u}} \otimes \boldsymbol{n}\mathrm{d}\Gamma &= \boldsymbol{0}.\end{aligned} \tag{43}$$

where $\boldsymbol{n}$ is the outward unit-normal vector to the microscopic boundary $\partial\Omega$ with an infinitesimal surface area $\mathrm{d}\Gamma$.

Constraints (40) can be applied by prescribing the respective fields at one point in the microscopic domain, along with the elimination of rigid body motion, to the corresponding macroscopic field values. To apply constraints (43), specific types of boundary conditions are used at the microscale. Typical choices for these boundary conditions are (i) zero fluctuation boundary conditions or (ii) periodic fluctuation boundary conditions as used later in this work.

Upscaling

Next, we discuss the upscaling relations which provide the constitutive equations for the macroscopic quantities. In computational homogenization, upscaling refers to the transfer of information from the microscale to the macroscale by requiring equality of the macroscopic and volume averaged microscopic (virtual) powers, known as the (extended) Hill–Mandel conditions in the literature [31,37,39]. The microscopic primary field ansatz e.g. (37) and (38), is then injected in the expression of the virtual power average and the macroscopic quantities are obtained by applying proper boundary conditions.

Mass diffusion The micro-macro scale equivalence of the virtual power due to mass diffusion

$$-\overline{\nabla}\delta\bar{\mu} \cdot \bar{\boldsymbol{j}} + \delta\bar{\mu}\dot{\bar{c}} = \Big\langle -\nabla\delta\mu \cdot \boldsymbol{j} + \delta\mu\dot{c}\Big\rangle. \tag{44}$$

Substituting the variation of the microscopic chemical potential $\delta\mu$ using (37) in the right hand side of (44) yields

$$-\overline{\nabla}\delta\bar{\mu} \cdot \bar{\boldsymbol{j}} + \delta\bar{\mu}\dot{\bar{c}} = \Big\langle -\overline{\nabla}\delta\bar{\mu} \cdot \boldsymbol{j} - \nabla\delta\tilde{\mu} \cdot \boldsymbol{j} + \delta\tilde{\mu}\dot{c} + \overline{\nabla}\delta\bar{\mu} \cdot (\boldsymbol{x} - \bar{\boldsymbol{x}})\dot{c} + \delta\bar{\mu}\dot{c}\Big\rangle. \tag{45}$$

Rearranging the above expression for $\delta\bar{\mu}$ and $\delta\tilde{\mu}$ yields

$$-\overline{\nabla}\delta\bar{\mu} \cdot \bar{\boldsymbol{j}} + \delta\bar{\mu}\dot{\bar{c}} = \Big\langle -\overline{\nabla}\delta\bar{\mu} \cdot [\boldsymbol{j} - \dot{c}(\boldsymbol{x} - \bar{\boldsymbol{x}})] + \delta\bar{\mu}\dot{c}\Big\rangle + \Big\langle -\nabla\delta\tilde{\mu} \cdot \boldsymbol{j} + \delta\tilde{\mu}\dot{c}\Big\rangle. \tag{46}$$

The last term in the above expression, after applying the chain rule and the divergence theorem, reflects the weak form of the microfluctuation mass conservation

$$\Big\langle -\nabla\delta\tilde{\mu} \cdot \boldsymbol{j} + \delta\tilde{\mu}\dot{c}\Big\rangle = \Big\langle \delta\tilde{\mu}(\nabla \cdot \boldsymbol{j} + \dot{c})\Big\rangle - \frac{1}{V}\int_{\partial\Omega} \delta\tilde{\mu}\boldsymbol{j} \cdot \boldsymbol{n}\,\mathrm{d}\Gamma. \tag{47}$$

The first term on the right hand side of the above expression is the weighted residual of the microscopic conservation of mass (34), whose solution at the microscale should vanish. For the prescribed zero microfluctuation boundary condition or the periodic boundary conditions, the second term also vanishes and Eq. (46) reduces to

$$-\overline{\nabla}\delta\bar{\mu}\cdot\bar{\boldsymbol{j}}+\delta\bar{\mu}\dot{\bar{c}}=-\overline{\nabla}\delta\bar{\mu}\cdot\left\langle\boldsymbol{j}-\dot{c}(\boldsymbol{x}-\bar{\boldsymbol{x}})\right\rangle+\delta\bar{\mu}\left\langle\dot{c}\right\rangle, \tag{48}$$

from where the macroscopic mass flux can be recognized as

$$\bar{\boldsymbol{j}}=\left\langle\boldsymbol{j}-\dot{c}(\boldsymbol{x}-\bar{\boldsymbol{x}})\right\rangle, \tag{49}$$

and the rate of change of the macroscopic concentration as

$$\dot{\bar{c}}=\left\langle\dot{c}\right\rangle. \tag{50}$$

The volume averages in Eqs. (49) and (50) can also be converted to boundary integrals using the divergence theorem and the microscopic mass conservation (34)

$$\bar{\boldsymbol{j}}=\frac{1}{V}\int_{\partial\Omega}j_n(\boldsymbol{x}-\bar{\boldsymbol{x}})\,\mathrm{d}\Gamma, \tag{51}$$

and

$$\dot{\bar{c}}=-\frac{1}{V}\int_{\partial\Omega}j_n\,\mathrm{d}\Gamma. \tag{52}$$

with $j_n=\boldsymbol{j}\cdot\boldsymbol{n}$ the normal outward mass flux.

Mechanics In the absence of inertia effects, the standard Hill–Mandel condition

$$\overline{\nabla}\delta\bar{\boldsymbol{u}}:\bar{\boldsymbol{\sigma}}=\left\langle\nabla\delta\boldsymbol{u}:\boldsymbol{\sigma}\right\rangle, \tag{53}$$

applies for the homogenization of the mechanical problem. Following similar steps as described above, allows identification of the (standard) macroscopic stress

$$\bar{\boldsymbol{\sigma}}=\left\langle\boldsymbol{\sigma}\right\rangle, \tag{54}$$

which can be converted to an expression in terms of tractions at the microscopic boundary

$$\bar{\boldsymbol{\sigma}}=\frac{1}{V}\int_{\partial\Omega}\boldsymbol{t}_n\otimes(\boldsymbol{x}-\bar{\boldsymbol{x}})\,\mathrm{d}\Gamma. \tag{55}$$

Once the solution to the microscopic problem (34) and (36) is known, the reaction mass fluxes j_n and the reaction forces $\boldsymbol{t}_n$ can be computed and post-processed to obtain the macroscopic quantities $\bar{\boldsymbol{j}}$, $\dot{\bar{c}}$ and $\bar{\boldsymbol{\sigma}}$. Next, we discuss the solution procedure to obtain the reaction fluxes j_n and forces $\boldsymbol{t}_n$ through a reduced order model, rather than the fully resolved model of the microscopic domain.

An alternative homogenization route is to average the dissipation, given in Eq. (7), at the microscale and equating it to an assumed macroscopic dissipation expression. For a first-order computational homogenization approach, the ansatz in Eqs. (40) and (43) can be inserted into the microscopic dissipation. Expanding and applying the required boundary conditions to eliminate the fluctuation fields, the corresponding macroscopic quantities can be obtained along with the weak forms of the balance laws at the microscale.

Model reduction leading to an enriched continuum

In this section, a model reduction of the microscopic coupled diffusion–mechanics problem is presented. The microscopic chemical potential and displacement fields are first decomposed into their steady-state and transient parts and reduced bases are identified.

The reaction fluxes and tractions, which are required to compute the macroscopic quantities, are written in terms of the coefficients of these reduced bases. Next, the expressions for the macroscopic quantities are derived explicitly. Finally, an emergent macroscopic enriched-continuum formulation, which arises as a consequence of model reduction at the microscale, is presented.

Finite element discretization

Using the finite element discretization, the linear momentum balance (36), the mass conservation (34) and the constitutive models (27)–(29), the discretized coupled diffusion–mechanics problem in terms of the unknown nodal values of the chemical potential $\underset{\sim}{\mu}$ and displacements $\boldsymbol{u}$ can be written as

$$\underline{K}_{\mu\mu}\underset{\sim}{\mu} + \underline{M}_{\mu\mu}\dot{\underset{\sim}{\mu}} + \underline{\boldsymbol{K}}_{\mu\boldsymbol{u}} \cdot \dot{\boldsymbol{u}} = -\underset{\sim}{j}_n, \tag{56}$$

$$\underline{\boldsymbol{K}}_{\boldsymbol{u}\mu}\underset{\sim}{\mu} + \underline{\boldsymbol{K}}_{\boldsymbol{u}\boldsymbol{u}} \cdot \boldsymbol{u} = \boldsymbol{t}_n, \tag{57}$$

where $\underline{K}_{\mu\mu}$, $\underline{M}_{\mu\mu}$, $\underline{\boldsymbol{K}}_{\boldsymbol{u}\boldsymbol{u}}$ and $\underline{\boldsymbol{K}}_{\boldsymbol{u}\mu}$ are the mobility, mass, stiffness and coupling matrices, respectively, and $\underline{\boldsymbol{K}}_{\mu\boldsymbol{u}} = -\left[\underline{\boldsymbol{K}}_{\boldsymbol{u}\mu}\right]^{\mathrm{T}}$. The right hand sides $\underset{\sim}{j}_n$ and $\boldsymbol{t}_n$ are the vector of reaction fluxes and reaction forces.

In the computational homogenization framework, once the solution for the microscopic primary fields $\underset{\sim}{\mu}$ and $\boldsymbol{u}$ is known, the reaction fluxes $\underset{\sim}{j}_n$ and reaction forces $\boldsymbol{t}_n$ can be computed. In a two-scale setting, this is an expensive task, especially in the transient regime, since it requires the solution of a coupled problem at each macroscopic material point at each time step. Hence, an approximate solution based on a model reduction technique is called for.

To apply the model reduction, instead of solving a coupled system of Eqs. (56)–(57), we first analyze each equation separately and then the coupling effect is taken into account when the reduced bases are constructed. The homogenization conditions in Eq. (40) amounts to kinematically constraint the microscale to the macroscopic point $\bar{\boldsymbol{x}}$ and requires the macroscopic chemical potential $\bar{\mu}$ to be the average value of the microscopic chemical potential field μ. In a discrete setting, it can be achieved by prescribing the microscopic fields μ and $\boldsymbol{u}$ degrees of freedom (DOF), at a point $\boldsymbol{x}$ in the microscopic domain, equal to the corresponding reference values of macroscopic fields $\bar{\mu}$ and $\bar{\boldsymbol{u}}$. It is allowed to fix the displacement field and the chemical potential at a point in the microscale because all the material properties i.e. $\mathbb{C}, \boldsymbol{S}, \boldsymbol{M}$ and Λ are independent of these solution fields. Also, the displacement field $\boldsymbol{u}$ at the microscale are defined up to the rigid body motion and the chemical potential μ can also be defined up to a constant since the microscopic flux $\boldsymbol{j}$, given in Eq. (15), depends on the gradient of chemical potential $\nabla\mu$ and linear momentum balance, given in Eq. (26), is not affected by adding a constant term to the chemical potential. In this study this point is chosen to be $\boldsymbol{x}_1$ which is at the lower left corner of the rectangular microscopic domain. The constraint (43) is satisfied by applying the periodic boundary conditions on the fluctuation fields $\tilde{\mu}$ and $\tilde{\boldsymbol{u}}$. Due to the applied periodicity, the DOFs at the other three corner nodes, denoted as points $\boldsymbol{x}_2, \boldsymbol{x}_3$ and $\boldsymbol{x}_4$, are also fully prescribed, while the rest of the DOFs in the microscopic domain are considered free. More details on applying the boundary conditions in a discrete setting for a scalar field like μ can be found in [31] and for a vector field like $\boldsymbol{u}$ in [32]. The discretized mass diffusion Eq. (56) partitioned into prescribed 'p' and free 'f' degree of freedoms takes the form

$$\begin{bmatrix} \underset{\sim}{K}_{\mu\mu}^{pp} & \underset{\sim}{K}_{\mu\mu}^{pf} \\ \underset{\sim}{K}_{\mu\mu}^{fp} & \underset{\sim}{K}_{\mu\mu}^{ff} \end{bmatrix} \begin{bmatrix} \underset{\sim}{\mu}^{p} \\ \underset{\sim}{\mu}^{f} \end{bmatrix} + \begin{bmatrix} \underset{\sim}{M}_{\mu\mu}^{pp} & \underset{\sim}{M}_{\mu\mu}^{pf} \\ \underset{\sim}{M}_{\mu\mu}^{fp} & \underset{\sim}{M}_{\mu\mu}^{ff} \end{bmatrix} \begin{bmatrix} \dot{\underset{\sim}{\mu}}^{p} \\ \dot{\underset{\sim}{\mu}}^{f} \end{bmatrix} + \begin{bmatrix} \underset{\sim}{\boldsymbol{K}}_{\mu\boldsymbol{u}}^{pp} & \underset{\sim}{\boldsymbol{K}}_{\mu\boldsymbol{u}}^{pf} \\ \underset{\sim}{\boldsymbol{K}}_{\mu\boldsymbol{u}}^{fp} & \underset{\sim}{\boldsymbol{K}}_{\mu\boldsymbol{u}}^{ff} \end{bmatrix} \cdot \begin{bmatrix} \dot{\underset{\sim}{\boldsymbol{u}}}^{p} \\ \dot{\underset{\sim}{\boldsymbol{u}}}^{f} \end{bmatrix} = \begin{bmatrix} -\underset{\sim}{j}_{n}^{p} \\ \underset{\sim}{\mathcal{Q}}^{f} \end{bmatrix}. \tag{58}$$

Similarly, the mechanical equation after partitioning into its prescribed and free DOF can be written as

$$\begin{bmatrix} \underset{\sim}{\boldsymbol{K}}_{\boldsymbol{u}\mu}^{pp} & \underset{\sim}{\boldsymbol{K}}_{\boldsymbol{u}\mu}^{pf} \\ \underset{\sim}{\boldsymbol{K}}_{\boldsymbol{u}\mu}^{fp} & \underset{\sim}{\boldsymbol{K}}_{\boldsymbol{u}\mu}^{ff} \end{bmatrix} \begin{bmatrix} \underset{\sim}{\mu}^{p} \\ \underset{\sim}{\mu}^{f} \end{bmatrix} + \begin{bmatrix} \underset{\sim}{\boldsymbol{K}}_{\boldsymbol{uu}}^{pp} & \underset{\sim}{\boldsymbol{K}}_{\boldsymbol{uu}}^{pf} \\ \underset{\sim}{\boldsymbol{K}}_{\boldsymbol{uu}}^{fp} & \underset{\sim}{\boldsymbol{K}}_{\boldsymbol{uu}}^{ff} \end{bmatrix} \cdot \begin{bmatrix} \underset{\sim}{\boldsymbol{u}}^{p} \\ \underset{\sim}{\boldsymbol{u}}^{f} \end{bmatrix} = \begin{bmatrix} \underset{\sim}{\boldsymbol{t}}_{n}^{p} \\ \underset{\sim}{\boldsymbol{\mathcal{Q}}}^{f} \end{bmatrix}. \tag{59}$$

For the microscopic response, both the chemical potential $\underset{\sim}{\mu}$ and displacement $\underset{\sim}{\boldsymbol{u}}$ are next split into their steady-state and transient parts.

Microscopic fields decomposition

According to the relaxed separation of scales, the transient response of the system evolves independently from the steady-state one. The steady-state response depends on the macroscopic input parameters ($\bar{\mu}$, $\bar{\boldsymbol{u}}$, $\overline{\nabla}\bar{\mu}$, and $\overline{\nabla}\bar{\boldsymbol{u}}$) through the prescribed DOFs $\underset{\sim}{\mu}^{p}$ and $\underset{\sim}{\boldsymbol{u}}^{p}$, whereas the transient response only affects the inclusions that are part of the free DOFs. (In a discrete setting this requires that the prescribed DOFs always reside in the matrix material so that the transient response can evolve independently.) Consequently, the free parts of the microscopic solution fields are decomposed into a steady-state and a transient part. The free part of the chemical potential field can be written as

$$\underset{\sim}{\mu}^{f} = \underset{\sim}{\mu}_{ss}^{f} + \underset{\sim}{\mu}_{tr}^{f}, \tag{60}$$

where $\underset{\sim}{\mu}_{ss}^{f}$ is the steady-state and $\underset{\sim}{\mu}_{tr}^{f}$ is the transient part. Since the mechanical response is coupled to that of the mass diffusion, the displacement field will also evolve in time due to the change of the chemical potential. The free part of the microscopic displacement field $\underset{\sim}{\boldsymbol{u}}^{f}$ is also decomposed into its steady-state $\underset{\sim}{\boldsymbol{u}}_{ss}^{f}$ and transient $\underset{\sim}{\boldsymbol{u}}_{tr}^{f}$ part

$$\underset{\sim}{\boldsymbol{u}}^{f} = \underset{\sim}{\boldsymbol{u}}_{ss}^{f} + \underset{\sim}{\boldsymbol{u}}_{tr}^{f}, \tag{61}$$

Next, the steady-state and transient reduced bases have to be determined for both the chemical and mechanical fields.

Steady-state response

The steady-state part of the microscale solution follows the macroscale solution instantaneously. To obtain the steady-state response, the discrete systems of Eqs. (58) and (59) are written considering the steady-state contributions $\underset{\sim}{\mu}_{ss}$ and $\underset{\sim}{\boldsymbol{u}}_{ss}$ only.

Mass diffusion

Substituting the steady-state chemical potential field μ_{ss} in the second line of Eq. (58) yields

$$\underset{\sim}{K}_{\mu\mu}^{fp}\, \underset{\sim}{\mu}^{p} + \underset{\sim}{K}_{\mu\mu}^{ff}\, \underset{\sim}{\mu}_{ss}^{f} + \underset{\sim}{M}_{\mu\mu}^{fp}\, \dot{\underset{\sim}{\mu}}^{p} + \underset{\sim}{M}_{\mu\mu}^{ff}\, \dot{\underset{\sim}{\mu}}_{ss}^{f} + \underset{\sim}{\boldsymbol{K}}_{\mu\boldsymbol{u}}^{fp} \cdot \dot{\underset{\sim}{\boldsymbol{u}}}^{p} + \underset{\sim}{\boldsymbol{K}}_{\mu\boldsymbol{u}}^{ff} \cdot \dot{\underset{\sim}{\boldsymbol{u}}}_{ss}^{f} = \underset{\sim}{\mathcal{Q}}^{f}. \tag{62}$$

Equation (62) is the evolution equation for μ_{ss}^{f}. Under the steady-state condition it holds that

$$\underset{\sim}{M}_{\mu\mu}^{fp}\, \dot{\underset{\sim}{\mu}}^{p} + \underset{\sim}{M}_{\mu\mu}^{ff}\, \dot{\underset{\sim}{\mu}}_{ss}^{f} + \underset{\sim}{\boldsymbol{K}}_{\mu\boldsymbol{u}}^{fp} \cdot \dot{\underset{\sim}{\boldsymbol{u}}}^{p} + \underset{\sim}{\boldsymbol{K}}_{\mu\boldsymbol{u}}^{ff} \cdot \dot{\underset{\sim}{\boldsymbol{u}}}_{ss}^{f} = \underset{\sim}{\mathcal{Q}}^{f}, \tag{63}$$

The steady-state part of the chemical potential $\underset{\sim}{\mu}_{ss}$ can then be expressed in terms of the prescribed DOF $\underset{\sim}{\mu}^{p}$ as

$$\underset{\sim}{\mu}^{f}_{ss} = \underline{S}^{fp}_{\mu\mu}\ \underset{\sim}{\mu}^{p}, \tag{64}$$

where $\underline{S}^{fp}_{\mu\mu} = -[\underline{K}^{ff}_{\mu\mu}]^{-1}\underline{K}^{fp}_{\mu\mu}$ is the Schur-complement. When multiplied with the macroscopic quantities $\underline{S}^{fp}_{\mu\mu}$ provides the steady-state homogenized response for the linear material model and thus can be considered as the steady-state reduced basis for the chemical potential field.

Mechanics

Similarly, to obtain the steady-state displacement field $\boldsymbol{\mu}^{f}_{ss}$ the second line of Eq. (59) is considered

$$\underline{\boldsymbol{K}}^{fp}_{\boldsymbol{u}\mu}\ \underset{\sim}{\mu}^{p} + \underline{\boldsymbol{K}}^{ff}_{\boldsymbol{u}\mu}\ \underset{\sim}{\mu}^{f}_{ss} + \underline{\boldsymbol{K}}^{fp}_{\boldsymbol{uu}} \cdot \boldsymbol{\mu}^{p} + \underline{\boldsymbol{K}}^{ff}_{\boldsymbol{uu}} \cdot \boldsymbol{\mu}^{f}_{ss} = \underline{\mathbf{0}}^{f}. \tag{65}$$

Substituting expression (64) for $\underset{\sim}{\mu}^{f}_{ss}$ in Eq. (65) yields

$$\underline{\boldsymbol{K}}^{fp}_{\boldsymbol{u}\mu}\ \underset{\sim}{\mu}^{p} + \underline{\boldsymbol{K}}^{ff}_{\boldsymbol{u}\mu}\underline{S}^{fp}_{\mu\mu}\ \underset{\sim}{\mu}^{p} + \underline{\boldsymbol{K}}^{fp}_{\boldsymbol{uu}} \cdot \boldsymbol{\mu}^{p} + \underline{\boldsymbol{K}}^{ff}_{\boldsymbol{uu}} \cdot \boldsymbol{\mu}^{f}_{ss} = \underline{\mathbf{0}}^{f}, \tag{66}$$

from where the expression for $\boldsymbol{\mu}^{f}_{ss}$ can be computed in terms of $\underset{\sim}{\mu}^{p}$ and $\boldsymbol{\mu}^{p}$

$$\boldsymbol{\mu}^{f}_{ss} = \underline{\boldsymbol{S}}^{fp}_{\boldsymbol{u}\mu}\ \underset{\sim}{\mu}^{p} + \underline{\boldsymbol{S}}^{fp}_{\boldsymbol{uu}} \cdot \boldsymbol{\mu}^{p}, \tag{67}$$

where $\underline{\boldsymbol{S}}^{fp}_{\boldsymbol{u}\mu} = -[\underline{\boldsymbol{K}}^{ff}_{\boldsymbol{uu}}]^{-1}\left(\underline{\boldsymbol{K}}^{fp}_{\boldsymbol{u}\mu} + \underline{\boldsymbol{K}}^{ff}_{\boldsymbol{u}\mu}\underline{S}^{fp}_{\mu\mu}\right)$ and $\underline{\boldsymbol{S}}^{fp}_{\boldsymbol{uu}} = -[\underline{\boldsymbol{K}}^{ff}_{\boldsymbol{uu}}]^{-1}\underline{\boldsymbol{K}}^{fp}_{\boldsymbol{uu}}$.

Transient response

As stated in "Microscopic fields decomposition" section , due to the relaxed separation of scales, to identify the transient reduced basis it is justified to use the free DOFs only. From Eq. (58) with account for (64), the free part of the discrete mass conservation equation can be written as

$$\underline{K}^{ff}_{\mu\mu}\ \underset{\sim}{\mu}^{f}_{tr} + \underline{M}^{ff}_{\mu\mu}\ \dot{\underset{\sim}{\mu}}^{f}_{tr} + \underline{\boldsymbol{K}}^{ff}_{\mu\boldsymbol{u}} \cdot \dot{\boldsymbol{u}}^{f}_{tr} = \underline{0}^{f}, \tag{68}$$

and from Eq. (59) with account for (65), the free part of the discrete conservation of linear momentum can be written as

$$\underline{\boldsymbol{K}}^{ff}_{\boldsymbol{u}\mu}\ \underset{\sim}{\mu}^{f}_{tr} + \underline{\boldsymbol{K}}^{ff}_{\boldsymbol{uu}} \cdot \boldsymbol{\mu}^{f}_{tr} = \underline{\mathbf{0}}^{f}, \tag{69}$$

from where

$$\boldsymbol{\mu}^{f}_{tr} = \underline{\boldsymbol{S}}^{ff}_{\boldsymbol{u}\mu}\ \underset{\sim}{\mu}^{f}_{tr}, \tag{70}$$

with $\underline{\boldsymbol{S}}^{ff}_{\boldsymbol{u}\mu} = -\left[\underline{\boldsymbol{K}}^{ff}_{\boldsymbol{uu}}\right]^{-1}\underline{\boldsymbol{K}}^{ff}_{\boldsymbol{u}\mu}$.

Assuming that the transient part of the microscopic solution fields, $\underset{\sim}{\mu}^{f}_{tr}$ and $\boldsymbol{\mu}^{f}_{tr}$, can be expressed in terms of a set of reduced basis functions, the transient chemical potential $\underset{\sim}{\mu}^{f}_{tr}$ is written in terms of these reduced basis functions Φ^{k}_{μ} and the corresponding coefficients η^{k}_{μ} as

$$\underset{\sim}{\mu}^{f}_{tr} \approx \sum_{k=1}^{N^{\mu}_{q}} \Phi^{k}_{\mu}\eta^{k}_{\mu} = \overset{*}{\underset{\sim}{\Phi}}_{\mu}\underset{\sim}{\eta}_{\mu}, \tag{71}$$

where $\underset{\sim}{\overset{*}{\Phi}}_{\mu}$ is the matrix containing the columns of the reduced transient functions Φ_{μ}^{k} and N_q^{μ} is the number of reduced basis functions for the chemical potential, which is much smaller than the total number of the free DOF N_f, i.e. $N_q^{\mu} \ll N_f$. Similarly, the transient displacement field $\boldsymbol{u}_{tr}$ can also be written in terms of the reduced basis functions $\boldsymbol{\Phi}_{\boldsymbol{u}}^{k}$ and their corresponding coefficients $\eta_{\boldsymbol{u}}^{k}$ as

$$\boldsymbol{u}_{tr}^{f} \approx \sum_{k=1}^{N_q^{\boldsymbol{u}}} \boldsymbol{\Phi}_{\boldsymbol{u}}^{k} \eta_{\boldsymbol{u}}^{k} = \underset{\sim}{\overset{*}{\boldsymbol{\Phi}}}_{\boldsymbol{u}} \underset{\sim}{\eta}_{\boldsymbol{u}}. \tag{72}$$

where $N_q^{\boldsymbol{u}}$ is the number of reduced basis for the displacement field. We will show later that N_q^{μ} and $N_q^{\boldsymbol{u}}$ and $\eta_{\boldsymbol{u}}$ and η_{μ} are the same. The selection criteria for the set of N_q basis functions will also be presented later. Next, the reduced basis functions in Eqs. (71) and (72) are identified using a spectral decomposition scheme.

Mass diffusion

Substituting $\boldsymbol{u}_{tr}^{f}$ from Eq. (70) into Eq. (68) provides

$$\underline{K}_{\mu\mu}^{ff} \underset{\sim}{\mu}_{tr}^{f} + \underline{\overset{\star}{M}}_{\mu\mu}^{ff} \dot{\underset{\sim}{\mu}}_{tr}^{f} = \underset{\sim}{0}^{f}, \tag{73}$$

where $\underline{\overset{\star}{M}}_{\mu\mu}^{ff} = \underline{M}_{\mu\mu}^{ff} + \underline{\boldsymbol{K}}_{\mu\boldsymbol{u}}^{ff} \underline{\boldsymbol{S}}_{\boldsymbol{u}\mu}^{ff}$ is the coupled mass matrix. The mass conservation (34) is a parabolic partial differential equation which has a natural solution that decays exponentially in time, i.e. $\underset{\sim}{\mu} = \Phi^{k} \exp(-\alpha^{k} t)$, substituting it in Eq. (73) yields the eigenvalue problems

$$(\underline{K}_{\mu\mu}^{ff} - \alpha^{k} \underline{\overset{\star}{M}}_{\mu\mu}^{ff}) \Phi^{k} = \underset{\sim}{0}^{f}, \tag{74}$$

where Φ^{k} is the k-th eigenvector and α^{k} the associated k-th eigenvalue. For the diffusion problem (34), the eigenvectors are the chemical potential distribution modes inside the domain and the corresponding eigenvalues are the inverse of a decay/rise time, i.e. $\tau^{k} = \frac{2\pi}{\alpha^{k}}$. Normalizing the eigenvectors Φ^{k} with respect to the mass matrix $\underline{\overset{\star}{M}}_{\mu\mu}^{ff}$,

$$\left[\Phi^{k}\right]^{\mathrm{T}} \underline{\overset{\star}{M}}_{\mu\mu}^{ff} \Phi^{k} = 1, \tag{75}$$

yields

$$\left[\Phi^{k}\right]^{\mathrm{T}} \underline{K}_{\mu\mu}^{ff} \Phi^{k} = \alpha^{k}. \tag{76}$$

The transient basis functions $\underset{\sim}{\overset{*}{\Phi}}_{\mu}$ in Eq. (71) can now be identified as the eigenvectors $\underset{\sim}{\overset{*}{\Phi}}$ obtained from the solution of the eigenvalue problem (74) i.e.

$$\underset{\sim}{\mu}_{tr}^{f} = \sum_{k=1}^{N_q} \Phi^{k} \eta_{k} = \underset{\sim}{\overset{*}{\Phi}} \underset{\sim}{\eta}, \tag{77}$$

where η^{k} can be interpreted as the modal amplitude, and $\underset{\sim}{\eta}$ is a column of size N_q.

Mechanics

Substituting the expression of $\underset{\sim}{\mu}_{tr}^{f}$ from Eqs. (77) in (70) provides the transient mechanical response

$$\boldsymbol{u}_{tr} = \sum_{k=1}^{N_q} \underline{\boldsymbol{S}}_{\boldsymbol{u}\mu}^{ff} \Phi^{k} \eta^{k} = \underline{\boldsymbol{S}}_{\boldsymbol{u}\mu}^{ff} \underset{\sim}{\overset{*}{\Phi}} \underset{\sim}{\eta}. \tag{78}$$

with $\underset{\sim}{\overset{*}{\Phi}}_{\boldsymbol{u}} = \underline{\boldsymbol{S}}_{\boldsymbol{u}\mu}^{ff} \underset{\sim}{\overset{*}{\Phi}}$. Next, we reconstruct the total solution for the chemical potential and displacement fields from their respective transient and steady-state responses.

Linear superposition

Substituting the expressions for $\underset{\sim}{\mu}_{ss}$ from (64) and $\underset{\sim}{\mu}_{tr}$ from (77) into (60), the total chemical potential field at the microscale can be written as

$$\underset{\sim}{\mu} = \underset{\sim}{\mu}_{ss} + \underset{\sim}{\mu}_{tr} = \underline{S}^{fp}_{\mu\mu}\, \underset{\sim}{\mu}^{p} + \overset{*}{\underline{\Phi}}\, \underset{\sim}{\eta}, \tag{79}$$

where only the reduced basis $\overset{*}{\underline{\Phi}}$ is coupled to the microscopic mechanical problem via the coupled mass matrix $\overset{\star}{\underline{M}}{}^{ff}_{\mu\mu}$ appearing in the eigenvalue problem (74).

Similarly, the total microscopic displacement field $\boldsymbol{\mu}$ can be reconstructed by substituting the expression for $\boldsymbol{\mu}_{ss}$ from (67) and $\boldsymbol{\mu}_{tr}$ from (78) into Eq. (61) i.e.

$$\boldsymbol{\mu} = \boldsymbol{\mu}_{ss} + \boldsymbol{\mu}_{tr} = \underline{\boldsymbol{S}}^{fp}_{\boldsymbol{u}\mu}\, \underset{\sim}{\mu}^{p} + \underline{\boldsymbol{S}}^{fp}_{\boldsymbol{u}\boldsymbol{u}} \cdot \boldsymbol{\mu}^{p} + \underline{\boldsymbol{S}}^{ff}_{\boldsymbol{u}\mu} \overset{*}{\underline{\Phi}}\, \underset{\sim}{\eta}. \tag{80}$$

Both, the steady-state and transient parts of the microscopic displacement field are coupled to the chemical problem as the coupling matrix $\underline{\boldsymbol{K}}_{\boldsymbol{u}\mu}$ appears in the matrices $\underline{\boldsymbol{S}}^{ff}_{\boldsymbol{u}\mu}$, $\underline{\boldsymbol{S}}^{ff}_{\boldsymbol{u}\mu}$ and $\overset{*}{\underline{\Phi}}$. Equations (79) and (80) shows that the microscopic solution fields, $\underset{\sim}{\mu}$ and $\boldsymbol{\mu}$, are completely given by the chemical potential $\underset{\sim}{\mu}^{p}$, the displacement $\boldsymbol{\mu}^{p}$ at the prescribed DOFs and the coefficients of the transient reduced basis $\underset{\sim}{\eta}$. Generally, in a two-scale setting, the microscopic fields at the prescribed DOFs, where the microfluctuations $\tilde{\mu}$ and $\tilde{\boldsymbol{u}}$ are zero, are given by the macroscopic quantities, as can be seen in Eqs. (37) and (38). Therefore, the only remaining unknown fields at the microscale are $\underset{\sim}{\eta}$ which can be obtained from the evolution equation, derived in the next subsection.

Evolution equation

The time evolution of $\underset{\sim}{\eta}$ can be obtained from the free part of Eq. (58)

$$\underline{K}^{fp}_{\mu\mu}\, \underset{\sim}{\mu}^{p} + \underline{K}^{ff}_{\mu\mu}\, \underset{\sim}{\mu}^{f} + \underline{M}^{fp}_{\mu\mu}\, \dot{\underset{\sim}{\mu}}^{p} + \underline{M}^{ff}_{\mu\mu}\, \dot{\underset{\sim}{\mu}}^{f} + \underline{\boldsymbol{K}}^{fp}_{\mu\boldsymbol{u}} \cdot \dot{\boldsymbol{\mu}}^{p} + \underline{\boldsymbol{K}}^{ff}_{\mu\boldsymbol{u}} \cdot \dot{\boldsymbol{\mu}}^{f} = \underset{\sim}{Q}^{f}, \tag{81}$$

Substituting the expressions for $\underset{\sim}{\mu}^{f}$ from Eq. (79) and $\boldsymbol{\mu}^{f}$ from Eqs. (80) into (81) and rearranging terms

$$\begin{aligned}
&(\underline{K}^{ff}_{\mu\mu} \overset{*}{\underline{\Phi}})\underset{\sim}{\eta} + (\underline{M}^{ff}_{\mu\mu} \overset{*}{\underline{\Phi}} + \underline{\boldsymbol{K}}^{ff}_{\mu\boldsymbol{u}} \underline{\boldsymbol{S}}^{ff}_{\boldsymbol{u}\mu} \overset{*}{\underline{\Phi}})\dot{\underset{\sim}{\eta}} \\
&\quad = -(\underline{K}^{fp}_{\mu\mu} + \underline{K}^{ff}_{\mu\mu} \underline{S}^{fp}_{\mu\mu})\, \underset{\sim}{\mu}^{p} \\
&\qquad -(\underline{M}^{fp}_{\mu\mu} + \underline{M}^{ff}_{\mu\mu} \underline{S}^{fp}_{\mu\mu} + \underline{\boldsymbol{K}}^{ff}_{\mu\boldsymbol{u}} \underline{\boldsymbol{S}}^{fp}_{\boldsymbol{u}\mu})\, \dot{\underset{\sim}{\mu}}^{p} - (\underline{\boldsymbol{K}}^{fp}_{\mu\boldsymbol{u}} + \underline{\boldsymbol{K}}^{ff}_{\mu\boldsymbol{u}} \underline{\boldsymbol{S}}^{fp}_{\boldsymbol{u}\boldsymbol{u}}) \cdot \dot{\boldsymbol{\mu}}^{p}.
\end{aligned} \tag{82}$$

Using the definition $\underline{S}^{fp}_{\mu\mu} = -\left[\underline{K}^{ff}_{\mu\mu}\right]^{-1} \underline{K}^{fp}_{\mu\mu}$, the first term on the right hand side of (82) drops out. Pre-multiplying the remaining equation with $[\overset{*}{\underline{\Phi}}]^{\mathrm{T}}$, Eq. (82) is written as

$$\begin{aligned}
&[\overset{*}{\underline{\Phi}}]^{\mathrm{T}} \underline{K}^{ff}_{\mu\mu} \overset{*}{\underline{\Phi}}\, \underset{\sim}{\eta} + [\overset{*}{\underline{\Phi}}]^{\mathrm{T}} \left(\underline{M}^{ff}_{\mu\mu} + \underline{\boldsymbol{K}}^{ff}_{\mu\boldsymbol{u}} \underline{\boldsymbol{S}}^{ff}_{\boldsymbol{u}\mu}\right) \overset{*}{\underline{\Phi}}\, \dot{\underset{\sim}{\eta}} \\
&\quad = -[\overset{*}{\underline{\Phi}}]^{\mathrm{T}} \left(\underline{M}^{fp}_{\mu\mu} + \underline{M}^{ff}_{\mu\mu} \underline{S}^{fp}_{\mu\mu} + \underline{\boldsymbol{K}}^{ff}_{\mu\boldsymbol{u}} \underline{\boldsymbol{S}}^{fp}_{\boldsymbol{u}\mu}\right)\, \dot{\underset{\sim}{\mu}}^{p} \\
&\qquad -[\overset{*}{\underline{\Phi}}]^{\mathrm{T}} \left(\underline{\boldsymbol{K}}^{fp}_{\mu\boldsymbol{u}} + \underline{\boldsymbol{K}}^{ff}_{\mu\boldsymbol{u}} \underline{\boldsymbol{S}}^{fp}_{\boldsymbol{u}\boldsymbol{u}}\right) \cdot \dot{\boldsymbol{\mu}}^{p},
\end{aligned} \tag{83}$$

which after using the normalization conditions in (75) and (76) takes the form

$$\underline{\alpha}\, \underset{\sim}{\eta} + \dot{\underset{\sim}{\eta}} = -\left(\overset{\star}{\underline{M}}{}^{qp}_{\mu\mu} \dot{\underset{\sim}{\mu}}^{p} + \overset{\star}{\underline{\boldsymbol{K}}}{}^{qp}_{\mu\boldsymbol{u}} \cdot \dot{\boldsymbol{\mu}}^{p}\right), \tag{84}$$

where

$$\begin{aligned}
\overset{\star}{\underline{M}}{}^{qp}_{\mu\mu} &= [\overset{*}{\underline{\Phi}}]^{\mathrm{T}} \left(\underline{M}^{fp}_{\mu\mu} + \underline{M}^{ff}_{\mu\mu} \underline{S}^{fp}_{\mu\mu} + \underline{\boldsymbol{K}}^{ff}_{\mu\boldsymbol{u}} \underline{\boldsymbol{S}}^{fp}_{\boldsymbol{u}\mu}\right), \\
\overset{\star}{\underline{\boldsymbol{K}}}{}^{qp}_{\mu\boldsymbol{u}} &= [\overset{*}{\underline{\Phi}}]^{\mathrm{T}} \left(\underline{\boldsymbol{K}}^{fp}_{\mu\boldsymbol{u}} + \underline{\boldsymbol{K}}^{ff}_{\mu\boldsymbol{u}} \underline{\boldsymbol{S}}^{fp}_{\boldsymbol{u}\boldsymbol{u}}\right).
\end{aligned} \tag{85}$$

Equation (84) is a set of N_q decoupled ordinary differential equations (ODEs) which represent the reduced order model for the evolution of diffusion–mechanics behavior at the microscale. The right hand side of (84) acts as the forcing term to the set of ODEs in terms of macroscopic fields present in $\underset{\sim}{\mu}^p$ and $\boldsymbol{u}^p$.

Reaction fluxes and forces

Next, we write the reaction mass fluxes $\underset{\sim}{j}_n^p$ and tractions $\underset{\sim}{\boldsymbol{t}}_n^p$ in terms of the coefficients of the steady-state and transient bases functions.

Reaction fluxes

The reaction mass fluxes $\underset{\sim}{j}_n^p$ can be obtained from the first line of the discrete mass conservation Eq. (58)

$$\underline{K}_{\mu\mu}^{pp}\,\underset{\sim}{\mu}^p + \underline{K}_{\mu\mu}^{pf}\,\underset{\sim}{\mu}^f + \underline{M}_{\mu\mu}^{pp}\,\dot{\underset{\sim}{\mu}}^p + \underline{M}_{\mu\mu}^{pf}\,\dot{\underset{\sim}{\mu}}^f + \underline{\boldsymbol{K}}_{\mu\boldsymbol{u}}^{pp}\cdot\dot{\boldsymbol{u}}^p + \underline{\boldsymbol{K}}_{\mu\boldsymbol{u}}^{pf}\cdot\dot{\boldsymbol{u}}^f = -\underset{\sim}{j}_n^p. \tag{86}$$

Substituting the expressions for $\underset{\sim}{\mu}^f$ and $\boldsymbol{u}^f$ from Eqs. (79) and (80) respectively yields

$$\begin{aligned}&\underline{K}_{\mu\mu}^{pp}\,\underset{\sim}{\mu}^p + \underline{K}_{\mu\mu}^{pf}\underline{S}_{\mu\mu}^{fp}\,\underset{\sim}{\mu}^p + \underline{K}_{\mu\mu}^{pf}\overset{*}{\underline{\Phi}}\,\underset{\sim}{\eta} + \underline{M}_{\mu\mu}^{pp}\,\dot{\underset{\sim}{\mu}}^p + \underline{M}_{\mu\mu}^{pf}\underline{S}_{\mu\mu}^{fp}\,\dot{\underset{\sim}{\mu}}^p + \underline{M}_{\mu\mu}^{pf}\overset{*}{\underline{\Phi}}\,\dot{\underset{\sim}{\eta}}\\ &+\underline{\boldsymbol{K}}_{\mu\boldsymbol{u}}^{pp}\cdot\dot{\boldsymbol{u}}^p + \underline{\boldsymbol{K}}_{\mu\boldsymbol{u}}^{pf}\underline{\boldsymbol{S}}_{\boldsymbol{u}\mu}^{fp}\,\dot{\underset{\sim}{\mu}}^p + \underline{\boldsymbol{K}}_{\mu\boldsymbol{u}}^{pf}\underline{\boldsymbol{S}}_{\boldsymbol{u}\boldsymbol{u}}^{fp}\cdot\dot{\boldsymbol{u}}^p + \underline{\boldsymbol{K}}_{\mu\boldsymbol{u}}^{pf}\underline{\boldsymbol{S}}_{\boldsymbol{u}\mu}^{ff}\overset{*}{\underline{\Phi}}\,\dot{\underset{\sim}{\eta}} = -\underset{\sim}{j}_n^p.\end{aligned} \tag{87}$$

Making use of $\underset{\sim}{\mu}^f = \overset{*}{\underline{\Phi}}\,\underset{\sim}{\eta}$ in the free part of the mass conservation Eq. (73), then pre-multiplying it with $\left[\underline{S}_{\mu\mu}^{fp}\right]^{\mathrm{T}}$ and using $\underline{S}_{\mu\mu}^{fp} = -\left[\underline{K}_{\mu\mu}^{ff}\right]^{-1}\underline{K}_{\mu\mu}^{fp}$, with account for the symmetry of $\underline{K}_{\mu\mu}$, replaces the third term $\underline{K}_{\mu\mu}^{pf}\overset{*}{\underline{\Phi}}\,\underset{\sim}{\eta}$ in Eq. (87) with $\left[\underline{S}_{\mu\mu}^{fp}\right]^{\mathrm{T}}\overset{\star}{\underline{M}}{}_{\mu\mu}^{ff}\overset{*}{\underline{\Phi}}\,\dot{\underset{\sim}{\eta}}$ i.e.

$$\begin{aligned}&\underline{K}_{\mu\mu}^{pp}\,\underset{\sim}{\mu}^p + \underline{K}_{\mu\mu}^{pf}\underline{S}_{\mu\mu}^{fp}\,\underset{\sim}{\mu}^p + \left[\underline{S}_{\mu\mu}^{fp}\right]^{\mathrm{T}}\overset{\star}{\underline{M}}{}_{\mu\mu}^{ff}\overset{*}{\underline{\Phi}}\,\dot{\underset{\sim}{\eta}} + \underline{M}_{\mu\mu}^{pp}\,\dot{\underset{\sim}{\mu}}^p + \underline{M}_{\mu\mu}^{pf}\underline{S}_{\mu\mu}^{fp}\,\dot{\underset{\sim}{\mu}}^p + \underline{M}_{\mu\mu}^{fp}\overset{*}{\underline{\Phi}}\,\dot{\underset{\sim}{\eta}}\\ &+\underline{\boldsymbol{K}}_{\mu\boldsymbol{u}}^{pp}\cdot\dot{\boldsymbol{u}}^p + \underline{\boldsymbol{K}}_{\mu\boldsymbol{u}}^{pf}\underline{\boldsymbol{S}}_{\boldsymbol{u}\mu}^{fp}\,\dot{\underset{\sim}{\mu}}^p + \underline{\boldsymbol{K}}_{\mu\boldsymbol{u}}^{pf}\underline{\boldsymbol{S}}_{\boldsymbol{u}\boldsymbol{u}}^{fp}\cdot\dot{\boldsymbol{u}}^p + \underline{\boldsymbol{K}}_{\mu\boldsymbol{u}}^{pf}\underline{\boldsymbol{S}}_{\boldsymbol{u}\mu}^{ff}\overset{*}{\underline{\Phi}}\,\dot{\underset{\sim}{\eta}} = -\underset{\sim}{j}_n^p.\end{aligned} \tag{88}$$

Now the steady-state constraint (63), projected onto the prescribed DOF, should be added to Eq. (88). For projecting the steady-state constraint (63) onto the prescribed DOF, it is first pre-multiplied with $\left[\underline{S}_{\mu\mu}^{fp}\right]^{\mathrm{T}}$, then the expressions of the steady-state chemical potential from (64) and the steady-state displacement field from (67) are substituted and finally the transpose of the whole expression is performed i.e.

$$\begin{aligned}&\underline{K}_{\mu\mu}^{pp}\,\underset{\sim}{\mu}^p + \underline{K}_{\mu\mu}^{pf}\underline{S}_{\mu\mu}^{fp}\,\underset{\sim}{\mu}^p + \left[\underline{S}_{\mu\mu}^{fp}\right]^{\mathrm{T}}\overset{\star}{\underline{M}}{}_{\mu\mu}^{ff}\overset{*}{\underline{\Phi}}\,\dot{\underset{\sim}{\eta}} + \underline{M}_{\mu\mu}^{pp}\,\dot{\underset{\sim}{\mu}}^p + \underline{M}_{\mu\mu}^{pf}\underline{S}_{\mu\mu}^{fp}\,\dot{\underset{\sim}{\mu}}^p + \underline{M}_{\mu\mu}^{fp}\overset{*}{\underline{\Phi}}\,\dot{\underset{\sim}{\eta}}\\ &+\underline{\boldsymbol{K}}_{\mu\boldsymbol{u}}^{pp}\cdot\dot{\boldsymbol{u}}^p + \underline{\boldsymbol{K}}_{\mu\boldsymbol{u}}^{pf}\underline{\boldsymbol{S}}_{\boldsymbol{u}\mu}^{fp}\,\dot{\underset{\sim}{\mu}}^p + \underline{\boldsymbol{K}}_{\mu\boldsymbol{u}}^{pf}\underline{\boldsymbol{S}}_{\boldsymbol{u}\boldsymbol{u}}^{fp}\cdot\dot{\boldsymbol{u}}^p + \underline{\boldsymbol{K}}_{\mu\boldsymbol{u}}^{pf}\underline{\boldsymbol{S}}_{\boldsymbol{u}\mu}^{ff}\overset{*}{\underline{\Phi}}\,\dot{\underset{\sim}{\eta}} + \underline{M}_{\mu\mu}^{pf}\underline{S}_{\mu\mu}^{fp}\,\dot{\underset{\sim}{\mu}}^p\\ &+\left[\underline{S}_{\mu\mu}^{fp}\right]^{\mathrm{T}}\underline{M}_{\mu\mu}^{ff}\underline{S}_{\mu\mu}^{fp}\,\dot{\underset{\sim}{\mu}}^p + \left[\underline{\boldsymbol{S}}_{\boldsymbol{u}\mu}^{fp}\right]^{\mathrm{T}}\underline{\boldsymbol{K}}_{\boldsymbol{u}\mu}^{ff}\underline{S}_{\mu\mu}^{fp}\,\dot{\underset{\sim}{\mu}}^p\\ &+\left[\left[\underline{\boldsymbol{K}}_{\mu\boldsymbol{u}}^{fp}\right]^{\mathrm{T}}\underline{S}_{\mu\mu}^{fp}\right]^{\mathrm{T}}\cdot\dot{\boldsymbol{u}}^p + \left[\left[\underline{\boldsymbol{S}}_{\boldsymbol{u}\boldsymbol{u}}^{fp}\right]^{\mathrm{T}}\underline{\boldsymbol{K}}_{\boldsymbol{u}\mu}^{ff}\underline{S}_{\mu\mu}^{fp}\right]^{\mathrm{T}}\cdot\dot{\boldsymbol{u}}^p = -\underset{\sim}{j}_n^p.\end{aligned} \tag{89}$$

Rearranging terms gives the resulting reaction mass flux

$$\underset{\sim}{j}_n^p = -\overset{\star}{\underline{M}}{}_{\mu\mu}^{pq}\,\dot{\underset{\sim}{\eta}} - \overset{\star}{\underline{K}}{}_{\mu\mu}^{pp}\,\underset{\sim}{\mu}^p - \overset{\star}{\underline{M}}{}_{\mu\mu}^{pp}\,\dot{\underset{\sim}{\mu}}^p - \overset{\star}{\underline{\boldsymbol{M}}}{}_{\mu\boldsymbol{u}}^{pp}\cdot\dot{\boldsymbol{u}}^p, \tag{90}$$

where

$$\begin{aligned}
\overset{\star}{\underline{M}}{}^{pq}_{\mu\mu} &= \left[\underline{S}^{fp}_{\mu\mu}\right]^{\mathrm{T}} \overset{\star}{\underline{M}}{}^{ff}_{\mu\mu} \overset{*}{\underline{\Phi}} + \underline{M}^{pf}_{\mu\mu} \overset{*}{\underline{\Phi}} + \underline{\boldsymbol{K}}^{pf}_{\mu\boldsymbol{u}} \underline{\boldsymbol{S}}^{ff}_{\boldsymbol{u}\mu} \overset{*}{\underline{\Phi}},\\
\overset{\star}{\underline{M}}{}^{pp}_{\mu\mu} &= \underline{M}^{pp}_{\mu\mu} + \underline{M}^{pf}_{\mu\mu} \underline{S}^{fp}_{\mu\mu} + \underline{M}^{pf}_{\mu\mu} \underline{S}^{fp}_{\mu\mu} + \left[\underline{S}^{fp}_{\mu\mu}\right]^{\mathrm{T}} \underline{M}^{ff}_{\mu\mu} \underline{S}^{fp}_{\mu\mu}\\
&\quad + \left[\underline{\boldsymbol{S}}^{fp}_{\boldsymbol{u}\mu}\right]^{\mathrm{T}} \underline{\boldsymbol{K}}^{ff}_{\boldsymbol{u}\mu} \underline{S}^{fp}_{\mu\mu} + \underline{\boldsymbol{K}}^{pf}_{\mu\boldsymbol{u}} \underline{\boldsymbol{S}}^{fp}_{\boldsymbol{u}\mu},\\
\overset{\star}{\underline{K}}{}^{pp}_{\mu\mu} &= \underline{K}^{pp}_{\mu\mu} + \underline{K}^{pf}_{\mu\mu} \underline{S}^{fp}_{\mu\mu},\\
\overset{\star}{\underline{\boldsymbol{M}}}{}^{pp}_{\mu\boldsymbol{u}} &= \underline{\boldsymbol{K}}^{pp}_{\mu\boldsymbol{u}} + \underline{\boldsymbol{K}}^{pf}_{\mu\boldsymbol{u}} \underline{\boldsymbol{S}}^{fp}_{\boldsymbol{u}\boldsymbol{u}} + \left[\left[\underline{\boldsymbol{K}}^{fp}_{\mu\boldsymbol{u}}\right]^{\mathrm{T}} \underline{S}^{fp}_{\mu\mu}\right]^{\mathrm{T}} + \left[\left[\underline{\boldsymbol{S}}^{fp}_{\boldsymbol{u}\boldsymbol{u}}\right]^{\mathrm{T}} \underline{\boldsymbol{K}}^{ff}_{\boldsymbol{u}\mu} \underline{S}^{fp}_{\mu\mu}\right]^{\mathrm{T}}.
\end{aligned} \tag{91}$$

Reaction Forces

Similarly, the first part of Eq. (59) provides the expression for the reaction forces $\underset{\sim}{\boldsymbol{t}}{}^{p}_{n}$ at the prescribed DOF

$$\underline{\boldsymbol{K}}^{pp}_{\boldsymbol{u}\mu}\, \underset{\sim}{\mu}{}^{p} + \underline{\boldsymbol{K}}^{pf}_{\boldsymbol{u}\mu}\, \underset{\sim}{\mu}{}^{f} + \underline{\boldsymbol{K}}^{pp}_{\boldsymbol{u}\boldsymbol{u}} \cdot \underset{\sim}{\boldsymbol{u}}{}^{p} + \underline{\boldsymbol{K}}^{pf}_{\boldsymbol{u}\boldsymbol{u}} \cdot \underset{\sim}{\boldsymbol{u}}{}^{f} = \underset{\sim}{\boldsymbol{t}}{}^{p}_{n}. \tag{92}$$

Substituting the expressions for $\underset{\sim}{\mu}{}^{f}$ and $\underset{\sim}{\boldsymbol{u}}{}^{f}$ from (79) and (80) into (92), gives

$$\begin{aligned}
&\underline{\boldsymbol{K}}^{pp}_{\boldsymbol{u}\mu}\, \underset{\sim}{\mu}{}^{p} + \underline{\boldsymbol{K}}^{pf}_{\boldsymbol{u}\mu} \underline{S}^{fp}_{\mu\mu}\, \underset{\sim}{\mu}{}^{p} + \underline{\boldsymbol{K}}^{pf}_{\boldsymbol{u}\mu} \overset{*}{\underline{\Phi}}\, \underset{\sim}{\eta} + \underline{\boldsymbol{K}}^{pp}_{\boldsymbol{u}\boldsymbol{u}} \cdot \underset{\sim}{\boldsymbol{u}}{}^{p}\\
&+ \underline{\boldsymbol{K}}^{pf}_{\boldsymbol{u}\boldsymbol{u}} \underline{\boldsymbol{S}}^{fp}_{\boldsymbol{u}\mu}\, \underset{\sim}{\mu}{}^{p} + \underline{\boldsymbol{K}}^{fp}_{\boldsymbol{u}\boldsymbol{u}} \underline{\boldsymbol{S}}^{fp}_{\boldsymbol{u}\boldsymbol{u}} \cdot \underset{\sim}{\boldsymbol{u}}{}^{p} + \underline{\boldsymbol{K}}^{pf}_{\boldsymbol{u}\boldsymbol{u}} \underline{\boldsymbol{S}}^{ff}_{\boldsymbol{u}\mu} \overset{*}{\underline{\Phi}}\, \underset{\sim}{\eta} = \underset{\sim}{\boldsymbol{t}}{}^{p}_{n},
\end{aligned} \tag{93}$$

which after rearranging for terms can be written as

$$\underset{\sim}{\boldsymbol{t}}{}^{p}_{n} = \overset{\star}{\underline{\boldsymbol{K}}}{}^{pq}_{\boldsymbol{u}\mu}\, \underset{\sim}{\eta} + \overset{\star}{\underline{\boldsymbol{K}}}{}^{pp}_{\boldsymbol{u}\mu}\, \underset{\sim}{\mu}{}^{p} + \overset{\star}{\underline{\boldsymbol{K}}}{}^{pp}_{\boldsymbol{u}\boldsymbol{u}} \cdot \underset{\sim}{\boldsymbol{u}}{}^{p}, \tag{94}$$

where

$$\begin{aligned}
\overset{\star}{\underline{\boldsymbol{K}}}{}^{pq}_{\boldsymbol{u}\mu} &= \underline{\boldsymbol{K}}^{pf}_{\boldsymbol{u}\mu} \overset{*}{\underline{\Phi}} + \underline{\boldsymbol{K}}^{pf}_{\boldsymbol{u}\boldsymbol{u}} \underline{\boldsymbol{S}}^{ff}_{\boldsymbol{u}\mu} \overset{*}{\underline{\Phi}},\\
\overset{\star}{\underline{\boldsymbol{K}}}{}^{pp}_{\boldsymbol{u}\mu} &= \underline{\boldsymbol{K}}^{pp}_{\boldsymbol{u}\mu} + \underline{\boldsymbol{K}}^{pf}_{\boldsymbol{u}\mu} \underline{S}^{fp}_{\mu\mu} + \underline{\boldsymbol{K}}^{pf}_{\boldsymbol{u}\boldsymbol{u}} \underline{\boldsymbol{S}}^{fp}_{\boldsymbol{u}\mu},\\
\overset{\star}{\underline{\boldsymbol{K}}}{}^{pp}_{\boldsymbol{u}\boldsymbol{u}} &= \underline{\boldsymbol{K}}^{pp}_{\boldsymbol{u}\boldsymbol{u}} + \underline{\boldsymbol{K}}^{pf}_{\boldsymbol{u}\boldsymbol{u}} \underline{\boldsymbol{S}}^{fp}_{\boldsymbol{u}\boldsymbol{u}}.
\end{aligned} \tag{95}$$

In the expressions of reaction fluxes (90) and reaction forces (94), the only unknown is $\underset{\sim}{\eta}$ which needs to be solved for in combination with the evolution Eq. (84), while $\underset{\sim}{\mu}{}^{p}$ and $\underset{\sim}{\boldsymbol{u}}{}^{p}$ are written in terms of the given (prescribed) macroscopic quantities.

Macroscopic quantities

Next, the expressions for the macroscopic quantities $\bar{\boldsymbol{\sigma}}$, $\bar{\boldsymbol{j}}$ and $\dot{\bar{c}}$ are derived in terms of macroscopic DOF, and the coefficients of the microscopic transient basis $\underset{\sim}{\eta}$.

Macroscopic flux

In the discretized form, the boundary integral (51) of the macroscopic flux $\bar{\boldsymbol{j}}$ can be written as

$$\bar{\boldsymbol{j}} = \frac{1}{V}\left[\Delta \underset{\sim}{\boldsymbol{x}}{}^{p}\right]^{\mathrm{T}} \underset{\sim}{j}{}^{p}_{n}, \tag{96}$$

where $\Delta \underset{\sim}{\boldsymbol{x}}{}^{p} = (\underset{\sim}{\boldsymbol{x}}{}^{p} - \underset{\sim}{I}{}^{p}\bar{\boldsymbol{x}})$, with $\underset{\sim}{I}{}^{p}$ is the column of ones with dimension $(p \times 1)$. Substituting the expression for $\underset{\sim}{j}{}^{p}_{n}$ from (90) in (96) gives

$$\bar{\boldsymbol{j}} = -\frac{1}{V}\left[\Delta \underset{\sim}{\boldsymbol{x}}{}^{p}\right]^{\mathrm{T}} \left(\overset{\star}{\underline{M}}{}^{pq}_{\mu\mu}\, \dot{\eta} + \overset{\star}{\underline{K}}{}^{pp}_{\mu\mu}\, \underset{\sim}{\mu}{}^{p} + \overset{\star}{\underline{M}}{}^{pp}_{\mu\mu}\, \dot{\underset{\sim}{\mu}}{}^{p} + \overset{\star}{\underline{\boldsymbol{M}}}{}^{pp}_{\mu\boldsymbol{u}} \cdot \dot{\underset{\sim}{\boldsymbol{u}}}{}^{p}\right), \tag{97}$$

which after substituting the discretized form of expression (37) for $\underset{\sim}{\mu}^p$ gives

$$\underset{\sim}{\mu}^p = \underset{\sim}{L}^p \bar{\mu} + \overline{\nabla}\bar{\mu} \cdot \Delta\underset{\sim}{\boldsymbol{x}}^p, \tag{98}$$

and (38) for $\underset{\sim}{\boldsymbol{\mu}}^p$ as

$$\underset{\sim}{\boldsymbol{\mu}}^p = \underset{\sim}{L}^p \bar{\boldsymbol{u}} + \overline{\nabla}\bar{\boldsymbol{u}} \cdot \Delta\underset{\sim}{\boldsymbol{x}}^p. \tag{99}$$

After rearranging terms, (97) takes the following form

$$\bar{\boldsymbol{j}} = \left[{}^1\underset{\sim}{\boldsymbol{M}}^{\dot{\eta}}\right]^{\mathrm{T}} \dot{\underset{\sim}{\eta}} + {}^2\boldsymbol{M}^{\overline{\nabla}\dot{\mu}} \cdot \overline{\nabla}\dot{\mu} + {}^1\boldsymbol{M}^{\dot{\mu}}\dot{\mu} + {}^2\boldsymbol{M}^{\overline{\nabla}\dot{\boldsymbol{u}}} : \left[\overline{\nabla}\dot{\boldsymbol{u}}\right]^{\mathrm{T}}. \tag{100}$$

where in the notation ${}^n\boldsymbol{A}^{\bullet}$, n is the tensorial order and $\bullet$ denotes the macroscopic quantity to which the coefficient $\boldsymbol{M}$ belongs to. The coefficients on the right hand side of Eq. (100) are given by

$$\begin{aligned}
\left[{}^1\underset{\sim}{\boldsymbol{M}}^{\dot{\eta}}\right]^{\mathrm{T}} &= -\frac{1}{V}\left[\Delta\underset{\sim}{\boldsymbol{x}}^p\right]^{\mathrm{T}} \overset{\star}{\underline{\underline{M}}}{}^{pq}_{\mu\mu}\,, && \text{(Row of } N_q \text{ 1st-order tensors (vectors))}\\
{}^2\boldsymbol{M}^{\overline{\nabla}\dot{\mu}} &= -\frac{1}{V}\left[\Delta\underset{\sim}{\boldsymbol{x}}^p\right]^{\mathrm{T}} \overset{\star}{\underline{\underline{K}}}{}^{pp}_{\mu\mu} \underline{\otimes} \Delta\underset{\sim}{\boldsymbol{x}}^p\,, && \text{(2nd-order tensor)}\\
{}^1\boldsymbol{M}^{\dot{\mu}} &= -\frac{1}{V}\left[\Delta\underset{\sim}{\boldsymbol{x}}^p\right]^{\mathrm{T}} \overset{\star}{\underline{\underline{M}}}{}^{pp}_{\mu\mu}\, \underset{\sim}{L}^p\,, && \text{(1st-order tensor)}\\
{}^2\boldsymbol{M}^{\overline{\nabla}\dot{\mu}} &= -\frac{1}{V}\left[\Delta\underset{\sim}{\boldsymbol{x}}^p\right]^{\mathrm{T}} \overset{\star}{\underline{\underline{M}}}{}^{pp}_{\mu\mu} \underline{\otimes} \Delta\underset{\sim}{\boldsymbol{x}}^p\,, && \text{(2nd-order tensor)}\\
{}^3\boldsymbol{M}^{\overline{\nabla}\dot{\boldsymbol{u}}} &= -\frac{1}{V}\left[\Delta\underset{\sim}{\boldsymbol{x}}^p\right]^{\mathrm{T}} \underline{\otimes} \overset{\star}{\underline{\underline{M}}}{}^{pp}_{\mu\boldsymbol{u}} \underline{\otimes} \Delta\underset{\sim}{\boldsymbol{x}}^p\,. && \text{(3rd-order tensor)}
\end{aligned} \tag{101}$$

where it has been taken into account that $\left[\Delta\underset{\sim}{\boldsymbol{x}}^p\right]^{\mathrm{T}} \overset{\star}{\underline{\underline{K}}}{}^{pp}_{\mu\mu}\, \underset{\sim}{L}^p = \left[\Delta\underset{\sim}{\boldsymbol{x}}^p\right]^{\mathrm{T}} \underline{\otimes} \overset{\star}{\underline{\underline{M}}}{}^{pp}_{\mu\boldsymbol{u}}\, \underset{\sim}{L}^p = \boldsymbol{0}$.

Macroscopic concentration rate

In its discrete form, the expression for the rate of change of the macroscopic concentration field $\dot{c}$, Eq. (52), can be written as

$$\dot{c} = -\frac{1}{V}\left[\underset{\sim}{L}^p\right]^{\mathrm{T}} \underset{\sim}{j}^p_n. \tag{102}$$

Substituting the expressions of $\underset{\sim}{\mu}^p$ and $\underset{\sim}{\boldsymbol{\mu}}^p$ from Eqs. (98) and (99) in Eq. (90) for $\underset{\sim}{j}^p_n$ respectively, and then rearranging terms in expression (102) gives

$$\dot{c} = \left[{}^0\underset{\sim}{\boldsymbol{C}}^{\dot{\eta}}\right]^{\mathrm{T}} \dot{\underset{\sim}{\eta}} + {}^0\boldsymbol{C}^{\dot{\mu}}\dot{\mu} + {}^1\boldsymbol{C}^{\overline{\nabla}\dot{\mu}} \cdot \overline{\nabla}\dot{\mu} + {}^2\boldsymbol{C}^{\overline{\nabla}\dot{\boldsymbol{u}}} : \left[\overline{\nabla}\dot{\boldsymbol{u}}\right]^{\mathrm{T}}, \tag{103}$$

where the coefficients on the right hand side of Eq. (103) are given by

$$\begin{aligned}
\left[{}^0\underset{\sim}{\boldsymbol{C}}^{\dot{\eta}}\right]^{\mathrm{T}} &= \frac{1}{V}\left[\underset{\sim}{L}^p\right]^{\mathrm{T}} \overset{\star}{\underline{\underline{M}}}{}^{pq}_{\mu\mu}\,, && \text{(Row of } N_q \text{ scalars)}\\
{}^0\boldsymbol{C}^{\dot{\mu}} &= \frac{1}{V}\left[\underset{\sim}{L}^p\right]^{\mathrm{T}} \overset{\star}{\underline{\underline{M}}}{}^{pp}_{\mu\mu}\, \underset{\sim}{L}^p\,, && \text{(Scalar)}\\
{}^1\boldsymbol{C}^{\overline{\nabla}\dot{\mu}} &= \frac{1}{V}\left[\underset{\sim}{L}^p\right]^{\mathrm{T}} \overset{\star}{\underline{\underline{M}}}{}^{pp}_{\mu\mu}\, \Delta\underset{\sim}{\boldsymbol{x}}^p\,, && \text{(1st-order tensor)}\\
{}^2\boldsymbol{C}^{\overline{\nabla}\dot{\boldsymbol{u}}} &= \frac{1}{V}\left[\underset{\sim}{L}^p\right]^{\mathrm{T}} \overset{\star}{\underline{\underline{M}}}{}^{pp}_{\mu\boldsymbol{u}} \underline{\otimes} \Delta\underset{\sim}{\boldsymbol{x}}^p\,, && \text{(2nd-order tensor)}
\end{aligned} \tag{104}$$

where $\left[\underset{\sim}{L}^p\right]^{\mathrm{T}} \overset{\star}{\underline{\underline{K}}}{}^{pp}_{\mu\mu}\, \underset{\sim}{L}^p = \left[\underset{\sim}{L}^p\right]^{\mathrm{T}} \overset{\star}{\underline{\underline{K}}}{}^{pp}_{\mu\mu}\, \Delta\underset{\sim}{\boldsymbol{x}}^p = \left[\underset{\sim}{L}^p\right]^{\mathrm{T}} \overset{\star}{\underline{\underline{M}}}{}^{pp}_{\mu\boldsymbol{u}}\, \underset{\sim}{L}^p = \boldsymbol{0}$ has been used.

Macroscopic stress

Similarly, the expression (55) for the macroscopic stress $\bar{\boldsymbol{\sigma}}$ in its discrete form can be written as

$$\bar{\boldsymbol{\sigma}} = \frac{1}{V}\left[\Delta \underset{\sim}{\boldsymbol{x}}^p\right]^{\mathrm{T}} \underline{\otimes} \underset{\sim}{\boldsymbol{t}}_n^p. \tag{105}$$

Substituting the expression for the reaction forces $\underset{\sim}{\boldsymbol{t}}_n^p$ from Eq. (94) provides

$$\bar{\boldsymbol{\sigma}} = \frac{1}{V}\left[\Delta \underset{\sim}{\boldsymbol{x}}^p\right]^{\mathrm{T}} \underline{\otimes} \left(\overset{\star}{\underline{\boldsymbol{K}}}{}^{pq}_{\boldsymbol{u}\mu}\, \underset{\sim}{\eta} + \overset{\star}{\underline{\boldsymbol{K}}}{}^{pp}_{\boldsymbol{u}\mu}\, \underset{\sim}{\mu}^p + \overset{\star}{\underline{\boldsymbol{K}}}{}^{pp}_{\boldsymbol{u}\boldsymbol{u}} \cdot \underset{\sim}{\boldsymbol{u}}^p\right), \tag{106}$$

which after using the discretized $\underset{\sim}{\mu}^p$ and $\underset{\sim}{\boldsymbol{u}}^p$ from Eqs. (98) and (99) take the following form

$$\bar{\boldsymbol{\sigma}} = {}^2\mathbb{C}^{\eta}\underset{\sim}{\eta} + {}^2\mathbb{C}^{\bar{\mu}}\bar{\mu} + {}^3\mathbb{C}^{\overline{\nabla}\bar{\mu}} \cdot \overline{\nabla}\bar{\mu} + {}^4\mathbb{C}^{\overline{\nabla}\bar{\boldsymbol{u}}} : \left[\overline{\nabla}\bar{\boldsymbol{u}}\right]^{\mathrm{T}}. \tag{107}$$

The coefficients in Eq. (107) are given by

$$\begin{aligned}
\left[{}^2\mathbb{C}^{\eta}\right]^{\mathrm{T}} &= \frac{1}{V}\left[\Delta \underset{\sim}{\boldsymbol{x}}^p\right]^{\mathrm{T}} \underline{\otimes} \overset{\star}{\underline{\boldsymbol{K}}}{}^{pq}_{\boldsymbol{u}\mu}\,, && \text{(Rows of } N_q \text{ 2nd-order tensors)}\\
{}^2\mathbb{C}^{\bar{\mu}} &= \frac{1}{V}\left[\Delta \underset{\sim}{\boldsymbol{x}}^p\right]^{\mathrm{T}} \underline{\otimes} \overset{\star}{\underline{\boldsymbol{K}}}{}^{pp}_{\boldsymbol{u}\mu}\, \underline{\boldsymbol{I}}^p\,, && \text{(2nd-order tensor)}\\
{}^3\mathbb{C}^{\overline{\nabla}\bar{\mu}} &= \frac{1}{V}\left[\Delta \underset{\sim}{\boldsymbol{x}}^p\right]^{\mathrm{T}} \underline{\otimes} \overset{\star}{\underline{\boldsymbol{K}}}{}^{pp}_{\boldsymbol{u}\mu} \underline{\otimes} \Delta \underset{\sim}{\boldsymbol{x}}^p\,, && \text{(3rd-order tensor)}\\
{}^4\mathbb{C}^{\overline{\nabla}\bar{\boldsymbol{u}}} &= \frac{1}{V}\left[\Delta \underset{\sim}{\boldsymbol{x}}^p\right]^{\mathrm{T}} \underline{\otimes} \overset{\star}{\underline{\boldsymbol{K}}}{}^{pp}_{\boldsymbol{u}\boldsymbol{u}} \underline{\otimes} \Delta \underset{\sim}{\boldsymbol{x}}^p\,, && \text{(4th-order tensor)}
\end{aligned} \tag{108}$$

where $\left[\Delta \underset{\sim}{\boldsymbol{x}}^p\right]^{\mathrm{T}} \underline{\otimes} \overset{\star}{\underline{\boldsymbol{K}}}{}^{pp}_{\boldsymbol{u}\boldsymbol{u}}\, \underset{\sim}{\boldsymbol{I}}^p = \boldsymbol{0}$ has been accounted for.

Mode selection criteria

The microscopic fields $\underset{\sim}{\mu}$ and $\underset{\sim}{\boldsymbol{u}}$, given by Eqs. (79) and (80), can be fully described by the macroscopic fields ($\bar{\mu}$, $\bar{\boldsymbol{u}}$), their gradients ($\overline{\nabla}\bar{\mu}$, $\overline{\nabla}\bar{\boldsymbol{u}}$) and the coefficients of the reduced bases $\underset{\sim}{\eta}$. The size of the original eigenvalue problem is equal to the number of free DOF N_f present in the system, which provides the complete set of eigenvectors $\underline{\Phi}$. Owing to the fact that in diffusion problems the lowest eigenvalues α^k are the most important ones, the eigenvectors corresponding to the first (several hundreds) lowest eigenvalues could be taken as the reduced basis. However, this would still entails a computationally inefficient scheme, since in a two-scale setting, where $\underset{\sim}{\eta}$ is solved at the macroscopic quadrature points as internal variables, solving hundreds of ordinary differential equations for the internal variables would still require noticeable computational efforts. Therefore, the reduced set of eigenvectors $\overset{*}{\underline{\Phi}}$ can be extracted from $\underline{\Phi}$ by taking into account that the right hand side of (84) acts as the forcing term and the modal coordinate η^k corresponding to the forcing terms with a higher magnitude will have a higher amplitude and therefore contribute more to the homogenized behavior at the macroscale. Substituting the expressions for the prescribed chemical potential $\underset{\sim}{\mu}^p$ and displacement $\underset{\sim}{\boldsymbol{u}}^p$ fields, Eqs. (98) and (99) , in the evolution Eq. (84) provides

$$\underline{\alpha}\,\underset{\sim}{\eta} + \dot{\underset{\sim}{\eta}} = -\left(\overset{\star}{\underline{M}}{}^{qp}_{\mu\mu}\left[\underline{\boldsymbol{I}}^p\dot{\mu} + \overline{\nabla}\dot{\mu}\cdot\Delta \underset{\sim}{\boldsymbol{x}}^p\right] + \overset{\star}{\underline{\boldsymbol{K}}}{}^{qp}_{\mu\boldsymbol{u}}\cdot\left[\underline{\boldsymbol{I}}^p\dot{\boldsymbol{u}} + \overline{\nabla}\dot{\boldsymbol{u}}\cdot\Delta \underset{\sim}{\boldsymbol{x}}^p\right]\right), \tag{109}$$

which after using the definition of the coupling terms in (101), (104) and (108) takes the following form

$$\underline{\alpha}\,\underset{\sim}{\eta} + \dot{\underset{\sim}{\eta}} = -\left({}^0\widehat{\mathbb{C}}^{\dot{\eta}}\dot{\mu} + \left[{}^1\widehat{\boldsymbol{M}}^{\dot{\eta}}\right]^{\mathrm{T}}\cdot\overline{\nabla}\dot{\mu} + \left[{}^2\widehat{\mathbb{C}}^{\eta}\right]^{\mathrm{T}} : \overline{\nabla}\dot{\boldsymbol{u}}\right), \tag{110}$$

where ${}^0\widehat{\underset{\sim}{\mathcal{C}}}^{\dot\eta} = V({}^0\underset{\sim}{\mathcal{C}}^{\dot\eta})$, ${}^1\widehat{\underset{\sim}{\boldsymbol{\mathcal{M}}}}^{\dot\eta} = V({}^1\underset{\sim}{\boldsymbol{\mathcal{M}}}^{\dot\eta})$ and ${}^2\underset{\sim}{\mathbb{C}}^{\eta} = V({}^2\widehat{\underset{\sim}{\mathbb{C}}}^{\eta})$, and takes into account that $\overset{\star}{\underline{\boldsymbol{K}}}{}^{qp}_{\mu\boldsymbol{\mu}}\underline{\boldsymbol{\mathcal{L}}}^{p} = \underline{\mathfrak{Q}}^{q}$. The coefficients ${}^0\underset{\sim}{\mathcal{C}}^{\dot\eta}$, ${}^1\underset{\sim}{\boldsymbol{\mathcal{M}}}^{\dot\eta}$ and ${}^2\underset{\sim}{\mathbb{C}}^{\eta}$ couple the microscopic transient behavior, in terms of η^k, to the macroscale fields. The higher the value of a coefficient, the higher the contribution of the respective η^k to the macroscale behavior. This information can be exploited to identify a reduced set of eigen vectors $\overset{*}{\underline{\Phi}}$. The eigenvectors associated to ${}^0C^{\dot\eta}_k$ with a relatively high contribution are identified using

$$E_{{}^0C^{\dot\eta}_k} = \frac{|{}^0\mathcal{C}^{\dot\eta}_k|}{\max\limits_k |{}^0C^{\dot\eta}_k|}, \tag{111}$$

where $|\bullet|$ is the absolute value of $\bullet$. Similarly, for each component of ${}^1\boldsymbol{M}^{\dot\eta}_k$ it can be stated

$$E_{{}^1\boldsymbol{M}^{\dot\eta}_k} = \frac{|{}^1\boldsymbol{M}^{\dot\eta}_k|}{\max\limits_k |{}^1\underset{\sim}{\boldsymbol{\mathcal{M}}}^{\dot\eta}_k|}, \tag{112}$$

and for each component of ${}^2\mathbb{C}^{\eta}_k$ using

$$E_{{}^2\mathbb{C}^{\eta}_k} = \frac{|{}^2\mathbb{C}^{\eta}_k|}{\max\limits_k |{}^2\underset{\sim}{\mathbb{C}}^{\eta}_k|}. \tag{113}$$

Then, a reduced eigenbasis $\overset{*}{\underline{\Phi}}$ can be obtained by requiring a minimum threshold $e_\bullet$ for a coefficient $\bullet$, such that

$$\begin{aligned}
\overset{*}{\underline{\Phi}}{}_{{}^0C^{\dot\eta}_k} &= \{\Phi^k \in \underline{\Phi} : E_{{}^0C^{\dot\eta}_k} \geq e_C\},\\
\overset{*}{\underline{\Phi}}{}_{{}^1\boldsymbol{M}^{\dot\eta}_k} &= \{\Phi^k \in \underline{\Phi} : E_{{}^1\boldsymbol{M}^{\dot\eta}_k} \geq e_{\boldsymbol{M}}\},\\
\overset{*}{\underline{\Phi}}{}_{{}^2\mathbb{C}^{\eta}_k} &= \{\Phi^k \in \underline{\Phi} : E_{{}^2\mathbb{C}^{\eta}_k} \geq e_{\mathbb{C}}\},\\
\overset{*}{\underline{\Phi}} &= \overset{*}{\underline{\Phi}}{}_{{}^0C^{\dot\eta}_k} \cup \overset{*}{\underline{\Phi}}{}_{{}^1\boldsymbol{M}^{\dot\eta}_k} \cup \overset{*}{\underline{\Phi}}{}_{{}^2\mathbb{C}^{\eta}_k}.
\end{aligned} \tag{114}$$

For a macroscopic simulation during an offline stage, individual threshold value signifies the corresponding macroscopic quantity and it should be selected accordingly.

Macroscale enriched continuum

The model reduction at the microscale leads to an enriched continuum formulation, as shown in Fig. 1c, at the macroscale with $\underset{\sim}{\eta}$ as the emergent (internal) variables and the set of Eq. (110) as their evolution equations. The developed reduced computational homogenization consists of two stages: an offline stage and an online stage. For a specific microstructure with given material properties and the finite element matrices [(Eqs. (56) and (57)], the offline stage consists of the solution of the eigenvalue problem (74), the selection of relevant eigenvectors using (114), and the computation of the coefficients for the macroscopic quantities (101), (104) and (108). Through the model reduction of the microscopic problem, (56)–(57), each macroscopic material point entails a set of N_q decoupled ordinary differential equations, which are inexpensive to solve. The evolution Eq. (110) are to be solved during the online stage along with the macroscopic conservation Eqs. (33) and (35), the constitutive equations obtained through the homogenization (100), (103) and (107). All together this constitutes the enriched coupled diffusion–mechanics continuum description as follows

Macroscopic mass conservation:	$\overline{\boldsymbol{\nabla}} \cdot \bar{\boldsymbol{j}} + \dot{\bar{c}} = 0,$
Macrocopic flux:	$\bar{\boldsymbol{j}} = \left[{}^{1}\underset{\sim}{\boldsymbol{M}}^{\dot{\eta}}\right]^{\mathrm{T}} \dot{\underset{\sim}{\eta}} + {}^{2}\boldsymbol{M}^{\overline{\nabla}\dot{\bar{\mu}}} \cdot \overline{\boldsymbol{\nabla}}\dot{\bar{\mu}} + {}^{1}\boldsymbol{M}^{\dot{\bar{\mu}}}\dot{\bar{\mu}} + {}^{2}\boldsymbol{M}^{\overline{\nabla}\dot{\bar{\boldsymbol{u}}}} \cdot \overline{\boldsymbol{\nabla}}\dot{\bar{\boldsymbol{u}}} + {}^{3}\boldsymbol{M}^{\overline{\nabla}\dot{\bar{\boldsymbol{u}}}} : \left[\overline{\boldsymbol{\nabla}}\dot{\bar{\boldsymbol{u}}}\right]^{\mathrm{T}},$
Macroscopic concentration rate:	$\dot{\bar{c}} = \left[{}^{0}\underset{\sim}{\boldsymbol{C}}^{\dot{\eta}}\right]^{\mathrm{T}} \dot{\underset{\sim}{\eta}} + {}^{0}\boldsymbol{C}^{\dot{\bar{\mu}}}\dot{\bar{\mu}} + {}^{1}\boldsymbol{C}^{\overline{\nabla}\dot{\bar{\mu}}} \cdot \overline{\boldsymbol{\nabla}}\dot{\bar{\mu}} + {}^{2}\boldsymbol{C}^{\overline{\nabla}\dot{\bar{\boldsymbol{u}}}} : \left[\overline{\boldsymbol{\nabla}}\dot{\bar{\boldsymbol{u}}}\right]^{\mathrm{T}},$
Macroscopic momentum conservation:	$\overline{\boldsymbol{\nabla}} \cdot \bar{\boldsymbol{\sigma}} = \boldsymbol{0},$
Macroscopic stress:	$\bar{\boldsymbol{\sigma}} = \left[{}^{2}\underset{\sim}{\mathbb{C}}^{\eta}\right]^{\mathrm{T}} \underset{\sim}{\eta} + {}^{2}\mathbb{C}^{\bar{\mu}}\bar{\mu} + {}^{3}\mathbb{C}^{\overline{\nabla}\bar{\mu}} \cdot \overline{\boldsymbol{\nabla}}\bar{\mu} + {}^{4}\mathbb{C}^{\overline{\nabla}\bar{\boldsymbol{u}}} : \left[\overline{\boldsymbol{\nabla}}\bar{\boldsymbol{u}}\right]^{\mathrm{T}},$
Internal variable evolution:	$\underset{\sim}{\alpha}\,\underset{\sim}{\eta} + \dot{\underset{\sim}{\eta}} = -\left({}^{0}\widehat{\underset{\sim}{\mathbb{C}}}^{\dot{\eta}}\dot{\bar{\mu}} + \left[{}^{1}\widehat{\underset{\sim}{\boldsymbol{M}}}^{\dot{\eta}}\right]^{\mathrm{T}} \cdot \overline{\boldsymbol{\nabla}}\dot{\bar{\mu}} + \left[{}^{2}\widehat{\underset{\sim}{\mathbb{C}}}^{\eta}\right]^{\mathrm{T}} : \overline{\boldsymbol{\nabla}}\dot{\bar{\boldsymbol{u}}}\right).$

Different solution methods can be adopted to solve the coupled diffusion–mechanics enriched continuum problem, depending on whether $\underset{\sim}{\eta}$ is evaluated at the macroscopic quadrature points, leading to an internal variable solution scheme, or at the nodes along with $\bar{\mu}$ and $\bar{\boldsymbol{u}}$, which leads to a multi-field solution scheme. Numerical analysis for the solution of the enriched continuum formulation will be discussed in a future contribution.

Numerical examples

In this section, the proposed reduced order homogenization for coupled transient diffusion–mechanics is analyzed at the microscale. First, the problem setting is presented. The coupled transient bases are identified. Then, the microscopic fields and macroscopic quantities computed with the reduced order homogenization are compared with those obtained through the expensive, fully resolved, conventional computational homogenization scheme. Finally, the computational efficiency of the proposed reduced order homogenization is assessed.

Problem setting

Lithium ion battery electrodes are majorly composed of two components: the electrolyte (matrix) and the active particles (inclusions). As an example, in this study a cathode–electrolyte system is considered, in which the electrolyte is lithium hexa-fluoro phosphate ($LiPF_6$) and the embedded active particles are made of lithium cobalt oxide ($LiCO_2$). For simplicity, it is assumed that the active particles are surrounded by the electrolyte only. All the other materials, e.g. the polymer binders, conductive particles etc., are disregarded following similar simplifications made in [30,40]. The material and geometric parameters are listed in Table 1. All material properties are assumed to be constant and do not change with the chemical potential or stresses in the material. For a given material, the chemical modulus Λ and the mobility coefficient M combine to form the diffusivity coefficient $\mathcal{D} = \Lambda M$ of the material. The diffusivity $\mathcal{D}_m$ of the lithium ions is much larger in the electrolyte as compared to the diffusivity $\mathcal{D}_i$ in the active particles, indicating that the relaxed separation of scales (32) holds for the considered problem. It is assumed that the electrolyte material does not swell with the introduction of lithium ions. The active particles are spherical in shape, vary in size and are placed randomly in the electrolyte which creates a poly-disperse heterogeneous medium [23]. In this example (for simplicity reasons), we consider a two dimensional mono-dispersed heterogeneous medium, as shown in Fig. 2, which is generated by a level set based random sequential adsorption method [41].

Table 1 Default parameters used in the simulation

Parameter	Symbol	Value	Units
RVE length	ℓ	1.0	(mm)
Inclusion diameter	ℓ_i	0.3	(mm)
Inclusion volume fraction	V_{f_i}	~ 0.5	
Maximum attainable concentration in inclusion [42]	$c_{\max}$	24,161	(mol m^{-3})
Minimum attainable concentration in inclusion [42]	$c_0 = 0.19c_{\max}$	4590.59	(mol m^{-3})
Absolute temperature	T_0	298	(K)
Boltzmann constant	k_b	1.3806×10^{-23}	(m^2 kg s^{-2} K^{-1})
Inclusion chemical modulus [28]	$\Lambda_i = k_b T_0/c_0$	10,202	(J m^{-3}/(mol m^{-3})^2)
Maximum chemical potential in inclusion	$\mu_{\max} = \Lambda_i(c_{\max} - c_0)$	1.99×10^8	(J /m^{-3}/(mol m^{-3}))
Matrix diffusivity [28]	$\mathcal{D}_m$	6×10^{-11}	(m^2 s^{-1})
Inclusion diffusivity [28]	$\mathcal{D}_i$	1×10^{-16}	(m^2 s^{-1})
Matrix characteristic time	$t_m = \frac{\ell^2}{\mathcal{D}_m}$	1.6×10^4	(s)
Inclusion characteristic time	$t_i = \frac{\ell_i^2}{\mathcal{D}_i}$	3×10^{12}	(s)
Matrix Young's modulus [42]	E_m	1	(GPa)
Inclusion Young's modulus [42]	E_i	10	(GPa)
Poisson's ratio [42]	ν_m & ν_i	0.3	
Inclusions partial molar volume [42]	γ	3.497×10^{-6}	(m^{-3} mol^{-1})
Number of elements		25,498 TRI3	
Number of nodes		12,494	
Total loading time	T	$0.1t_i$	(s)
Loading frequency	ω	1	(Hz)

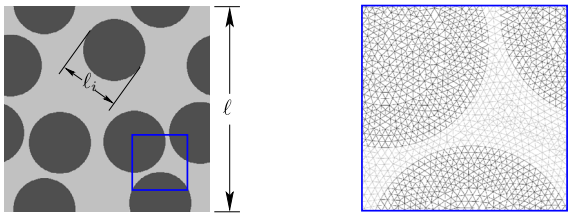

Fig. 2 **a** Two dimensional representation of a lithium ion battery cathode–electrolyte system with mono-dispersed circular active particles (inclusions); ℓ is the characteristic size of the RVE and ℓ_i is the diameter of the inclusions. **b** A fragment of the finite element mesh corresponding to the area indicated by the box in **a**. The full FE mesh consists of 25,498 linear triangular elements and 12,494 nodes

In the simulations, all the parameters were non-dimensionalized, the time was normalized with respect to the characteristic diffusion time of the inclusion, i.e. $\hat{t} = \frac{t}{t_i}$, the lengths are normalized with respect to the characteristic length of the microscopic domain, i.e. $\hat{x} = \frac{x}{\ell}$, the chemical potential is normalized with respect to the maximum attainable chemical potential in the inclusion $\hat{\mu} = \frac{\mu}{\mu_{\max}}$, where $\mu_{\max} = \Lambda_i(c_{\max} - c_0)$, the displacement field is normalized with respect to the characteristic length of the microscopic domain, i.e. $\hat{\boldsymbol{u}} = \frac{\boldsymbol{u}}{\ell}$ and the stresses are normalized with respected to the Young's modulus of the inclusion E_i.

The microscopic domain is excited by the chemical loading given in terms of the macroscopic chemical potential $\bar{\mu}$ and the gradient of the macroscopic chemical potential $\overline{\nabla}\bar{\mu}$ as a function of time i.e.

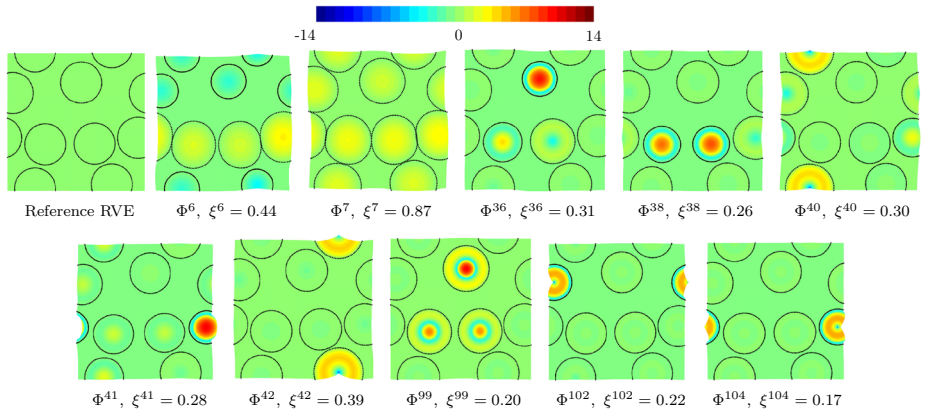

Fig. 3 Eigenvectors $\overset{*}{\underline{\Phi}}_{\mu}$ and $\overset{*}{\underline{\Phi}}_{\boldsymbol{u}}$ are shown in a coupled manner: the color map indicates the chemical potential value and the corresponding mechanical modes are indicated by the geometry change (swelling or shrinkage) of the inclusions. The displacement field is scaled 5 times relative to the reference configuration. The quantitative contribution ξ^k of the mode is defined in Eq. (116)

$$\begin{aligned} \bar{\mu}(t) &= \bar{\mu} \sin \omega t\,, \\ \overline{\nabla}\bar{\mu}(t) &= \overline{\nabla}\bar{\mu} \sin \omega t\,, \end{aligned} \tag{115}$$

where $\omega = \frac{2\pi}{T}$ is the angular loading frequency, T is the time of one period and $\bar{\mu} = \mu_{\max}$ and $\overline{\nabla}\bar{\mu} = 0.1\mu_{\max}$ are assumed. Externally applied mechanical loads to the microscale are neglected here. At the microscale, periodic boundary conditions are used to satisfy the Hill-Mandel conditions for both the mass diffusion and mechanical problems. The microscopic domain, shown in Fig. 2b, is discretized with linear triangular finite elements. For time integration, the backward-Euler method was used with a time step $\Delta t = 1 \times 10^{-3} T$[s].

Reduced basis identification

After assembling the finite element matrices and applying the boundary conditions at the microscale, the first step of the reduced order homogenization is the solution of the coupled eigenvalue problem (74). This eigenvalue problem is solved for the first two hundred smallest eigenvalues and the corresponding eigenvectors $\underline{\Phi}$. Then, using the mode selection criteria given by Eq. (114), the reduced basis $\overset{*}{\underline{\Phi}} \in \underline{\Phi}$ is based on the coupling terms ${}^0C_k^{\dot{\eta}}$, ${}^1\boldsymbol{M}_k^{\dot{\eta}}$ and ${}^2\mathbb{C}_k^{\eta}$ with the threshold value $e_C = e_{\boldsymbol{M}} = e_{\mathbb{C}} = 0.1$. The number of eigenvectors selected in the eigenbasis $\overset{*}{\underline{\Phi}}$ depends on the topology of the micro-structure, the strength of the coupling in diffusion–mechanics and the material contrast between the matrix and the inclusions. For each selected eigenvector Φ_{μ}^k, there is a corresponding coupled mechanical eigenvector $\boldsymbol{\Phi}_{\boldsymbol{u}}^k = \underline{\boldsymbol{S}}_{\boldsymbol{u}\mu}^{ff} \Phi_{\mu}^k$, both $\overset{*}{\underline{\Phi}}_{\mu}$ and $\overset{*}{\underline{\boldsymbol{\Phi}}}_{\boldsymbol{u}}$ are shown for the considered micro-structure in a coupled manner in Fig. 3. The ten modes selected are not the modes corresponding to the 10 consecutive smallest eigenvalues.

The inclusions swell where the chemical potential is high, indicated by the red regions inside the domain and the inclusions shrink where the chemical potential is low, indicated by the blue regions. The modes have contributions in the inclusions only, in accordance with the relaxed separation of scales. If the material properties do not fulfill the requirements of relaxed separation of scales (32) then the eigenvectors might have contributions

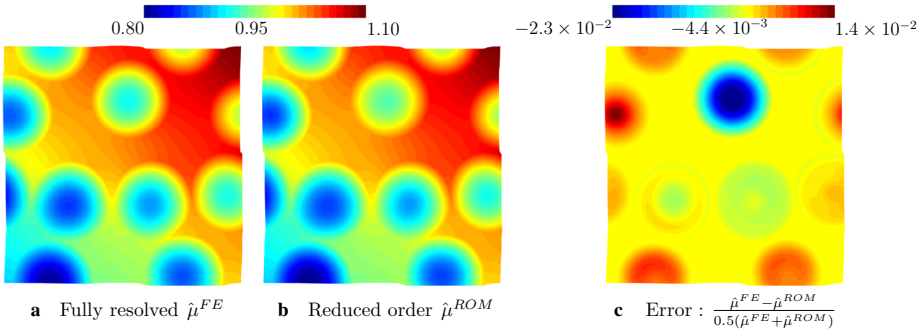

Fig. 4 Chemical potential field $\hat{\mu} = \mu/\mu_{\max}$ in the microscopic domain at time step $\hat{t} = 250\Delta\hat{t}$. **a** Fully resolved finite element solution $\hat{\mu}^{FE}$ **b** reduced order solution $\hat{\mu}^{ROM}$ and **c** the relative error with respect to their average $\frac{\hat{\mu}^{FE}-\hat{\mu}^{ROM}}{0.5(\hat{\mu}^{FE}+\hat{\mu}^{ROM})}$

in the matrix and consequently the proposed reduced homogenization method will not capture the phenomena adequately.

Among the selected eigenvectors, shown in Fig. 3, there is one eigenvector with the highest relative importance of the eigenmodes in terms of their contribution to the macroscale, which can be quantified by a measure ξ^k

$$\xi^k = \frac{1}{3}\left(\frac{|{}^0\boldsymbol{C}_k^{\dot{\eta}}|}{\max\limits_k|{}^0\boldsymbol{C}_k^{\dot{\eta}}|} + \frac{||{}^1\boldsymbol{M}_k^{\dot{\eta}}||}{\max\limits_k||{}^1\boldsymbol{M}_k^{\dot{\eta}}||} + \frac{||{}^2\mathbb{C}_k^{\eta}||}{\max\limits_k||{}^2\mathbb{C}_k^{\eta}||}\right), \tag{116}$$

where $|\bullet|$ and $||\bullet||$ are the absolute value and Frobenius norm of a quantity $\bullet$. In this example, eigenvector numbered 7 has the highest contribution to the macroscale, while other eigenvectors in $\underset{\sim}{\overset{*}{\Phi}}$ make only small improvements in capturing the phenomena. For a more detailed mode selection analysis, in the case of heat diffusion, the reader is referred to [31].

Microscale simulations

Next, we compare the microscopic fields computed by the model reduction method and the (expensive) fully resolved finite element calculations. For the fully resolved finite element analysis, the coupled system of Eqs. (56)–(57) is solved for $\underset{\sim}{\mu}$ and $\boldsymbol{\mu}$, directly on the finite element mesh of the considered RVE 2b. For the reduced model, the coefficients $\underset{\sim}{\eta}$ are solved by using Eq. (110); subsequently, the microscopic fields $\underset{\sim}{\mu}$ and $\boldsymbol{\mu}$, are reconstructed (localization operation) by post-processing through Eqs. (79) and (80), respectively. Note that, in a two-scale simulation the post-processing of microscopic fields $\underset{\sim}{\mu}$ and $\boldsymbol{\mu}$, is generally not done, unless the microscopic fields are also the quantities of interest in addition to the macroscopic field. Figure 4 shows the contour plots of the normalized chemical potential $\hat{\mu}$ and Fig. 5 shows the contour plots of the normalized hydrostatic stress $\hat{\sigma}_{hyd} = \frac{\hat{\sigma}_{11}+\hat{\sigma}_{22}}{3}$ at time $\hat{t} = 250\Delta\hat{t}$.

The minor differences between the fully resolved solution and the reduced order model are due to the approximate nature of the model reduction.

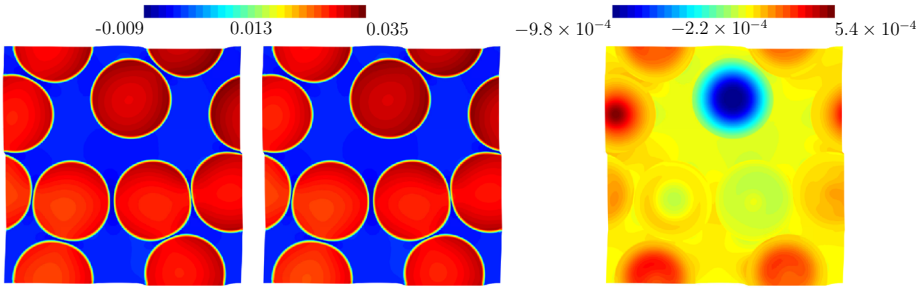

Fig. 5 Hydrostatic stress $\hat{\sigma}_{hyd} = \frac{\hat{\sigma}_{11}+\hat{\sigma}_{22}}{3}$ induced at the microscale due to diffusion mechanical coupling at time $\hat{t} = 250\Delta\hat{t}$. **a** Fully resolved finite element solution $\hat{\sigma}^{FE}_{hyd}$ **b** reduced order solution $\hat{\sigma}^{ROM}_{hyd}$ and **c** the relative error with respect to their average $\frac{\hat{\sigma}^{FE}_{hyd}-\hat{\sigma}^{ROM}_{hyd}}{0.5(\hat{\sigma}^{FE}_{hyd}+\hat{\sigma}^{ROM}_{hyd})}$

Effective macroscopic quantities

Next, we compare the macroscopic quantities $\bar{\boldsymbol{j}}$, $\dot{\bar{c}}$, $\bar{\boldsymbol{\sigma}}$ computed with the conventional transient homogenization and the developed reduced order homogenization. For conventional computational homogenization, the fully resolved finite element analysis of the coupled system of Eqs. (56)–(57) is performed and then the macroscopic flux $\bar{\boldsymbol{j}}$ is computed using (96), the macroscopic concentration rate $\dot{\bar{c}}$ using (102) and the macroscopic stress $\bar{\boldsymbol{\sigma}}$ using (105), where the reaction fluxes $\underset{\sim}{j}^p_n$ and the reaction forces $\underset{\sim}{\boldsymbol{t}}^p_n$ are post-processed using the expressions in (86) and (92), respectively. For the reduced model calculations, the eigenvalue problem (74) is solved in the offline stage and the coupling terms in (101), (104) and (108) are calculated and stored. During the online stage, the evolution Eq. (110) is solved for $\underset{\sim}{\eta}$. Once $\underset{\sim}{\eta}$ is known, the macroscopic quantities are calculated directly from the expressions (100), (103) and (107) for the macroscopic mass flux $\bar{\boldsymbol{j}}$, the macroscopic concentration rate $\dot{\bar{c}}$ and the macroscopic stress $\bar{\boldsymbol{\sigma}}$, respectively. Figure 6 shows the time evolution of the macroscopic quantities computed with the (expensive) conventional transient computational homogenization (CTH) method (shown in red) and the proposed inexpensive reduced computational homogenization (RTH) method (shown in blue). The reduced order homogenization method shows an excellent approximation without any noticeable discrepancies.

The computational gains achieved with the reduced model are substantial. Neglecting the off-line stage, motivated by the fact that for a specific microstructure and set of material parameters the off-line stage only needs to be performed once. Using Matlab 2018b on a computer with Core-i7 4.4 GHz processor and 16Gb memory, for the conventional computational homogenization the coupled problem (56)–(57) takes approximately 5000 times more computational time than the solution of the uncoupled ordinary differential Eq. (110). Next, we asses the proposed reduced model with different value of coupling coefficient γ and the microscopic domain size ℓ.

Diffusion–mechanics coupling effect

In diffusion–mechanics, the coupling is governed by the partial molar volume parameter γ in Eq. (28). The higher the value of γ, the higher the coupling will be. The constitutive Eq. (23) has an upper limit of applicability since the effective elastic tensor $\overset{*}{\mathbb{C}} = \left(\mathbb{C} - \frac{\boldsymbol{S}\otimes\boldsymbol{S}}{\Lambda}\right)$

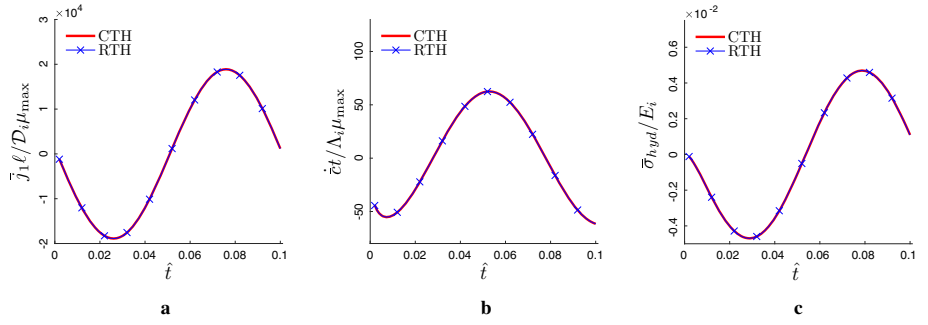

Fig. 6 Comparison between the macroscopic quantities computed with the conventional computational homogenization (based on the fully resolved microscale RVE analysis), shown in red, and the reduced order homogenization, shown in blue. **a** Macroscopic mass flux $\bar{j}_1$ in $\boldsymbol{x}_1$ direction, **b** macroscopic concentration rate $\dot{\bar{c}}$ and **c** macroscopic hydrostatic stress $\bar{\sigma}_{hyd} = \frac{\bar{\sigma}_{11}+\bar{\sigma}_{22}}{3}$

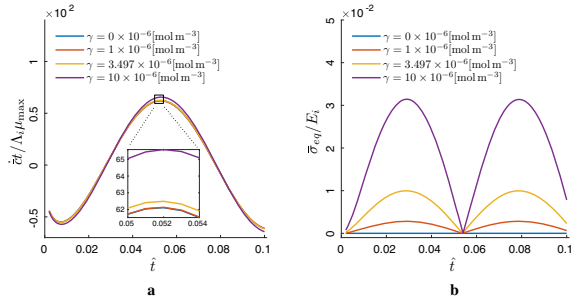

Fig. 7 The effect of the coupling term γ on **a** the macroscopic rate term $\dot{\bar{c}}$ and **b** the macroscopic equivalent stress $\bar{\sigma}_{eq}$. The equivalent stress is calculated as $\bar{\sigma}_{eq} = \sqrt{\bar{\sigma}_{11}^2 + \bar{\sigma}_{22}^2 + 2\bar{\sigma}_{12}^2}$

can become non-positive definite, which will make the eigenvalues ϱ (76) equal to zero or even negative. However, for the realistic material properties of the cathode in lithium ion batteries, this is not a problem since the upper limit for γ is 21×10^{-6}(mol m^{-3}), which is much greater than the physical value of $\gamma = 3.497 \times 10^{-6}$(mol m^{-3}). Figure 7 shows the effect of increasing the γ value. The macroscopic rate term $\dot{\bar{c}}$ and the macroscopic stress $\bar{\boldsymbol{\sigma}}$ increase as γ increases in accordance with their microscopic counterparts (23) and (24), respectively.

The proposed model reduction scheme captures the full finite element solution very well, and hence for clarity the finite element solution is not shown anymore. Next, we analyze the effect of the microscopic domain size on the macroscopic quantities.

Size effect

To measure microscopic size effect on the macroscopic quantities, the material parameters are kept the same and the characteristic size of the microscopic domain ℓ is changed while keeping the inclusions size ℓ_i the same or scaling it along with the microscopic size. In the first case, the macroscopic quantities do not vary with the changing RVE size. However, if the inclusions size ℓ_i is scaled along with the characteristic microscopic size ℓ the microscopic and the macroscopic quantities change. For the later case, the normalized characteristic length of the microscale is changed from $\hat{\ell} = 1 \times 10^{-2}$ to $\hat{\ell} = 1 \times 10^{1}$ and

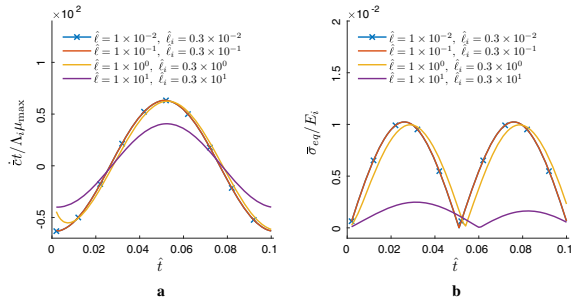

Fig. 8 Influence of the microscopic characteristic length scale $\hat{\ell}$ on **a** the macroscopic concentration rate $\dot{\bar{c}}$ and **b** the equivalent macroscopic stress $\bar{\sigma}_{eq}$

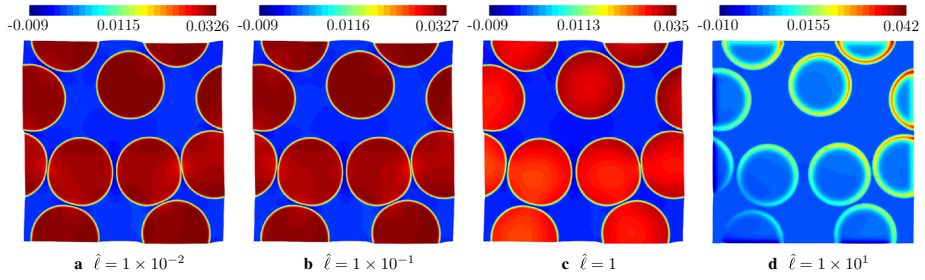

Fig. 9 Hydrostatic stress field $\hat{\sigma}_{hyd} = \frac{\hat{\sigma}_{11}+\hat{\sigma}_{22}}{3}$ at the microscale with different microscopic sizes $\hat{\ell}$

accordingly the inclusion characteristic length from $\hat{\ell}_i = 0.3 \times 10^{-2}$ to $\hat{\ell}_i = 0.3 \times 10^{1}$, respectively. As expected, for the smaller microstructures (up to $\hat{\ell} = 1 \times 10^{-1}$ with $\hat{\ell}_i = 0.3 \times 10^{-1}$), due to almost instantaneous mass diffusion in the inclusion at the microscale, the averaged macroscopic transient effects are negligible as compared to the transient effects computed with a larger unit-cell, as can be seen in Fig. 8a.

For the larger microstructural sizes the response is clearly size dependent. In particular, the macroscopic stresses $\bar{\boldsymbol{\sigma}}$ are much higher for small microstructures compared to the large ones. This is due to the coupling effect and the diffusion rate. For smaller sizes, the chemical potential (and the concentration of a species) increases in the inclusion domain, which causes the inclusions to swell and produce higher stresses on average. Conversely, when the microscale size is increased, within the same time period, the mass diffusion happens to the outer layer of the inclusions, swelling only that part of the inclusions, which creates higher local stresses, as can be seen in Fig. 9. However, due to overall increase in the volume of the microscopic domain and the small relative volume of high stress regions, the macroscopic volume average stresses decrease, as can be observed in Fig. 8.

Conclusions

In this work, a model reduction based homogenization technique for coupled diffusion–mechanics problems has been presented. A formulation based on the chemical potential and linear strain field is derived, which eases the implementation since it only requires a C^0-continuous discretization. This is in contrast with the conventional formulation used in diffusion–mechanics based on the concentration and strain fields, which requires a

less convenient C^1-continuous finite element formulation. For the homogenization of the coupled diffusion–mechanics, the equivalence of the virtual power for mass diffusion (extended Hill–Mandel condition), and the virtual work of internal forces (standard Hill–Mandel condition) are used for the diffusion and mechanical problems, respectively. A model reduction technique, inspired by the dynamic mode synthesis approach, is developed for the coupled system of equations relying on the linearity of the problem and the relaxed separation of scales. Accordingly, both the microscopic chemical potential and displacement fields are split into their steady-state and transient parts. Using static condensation, a reduced basis is first identified for the steady-state fields. Then for the transient part, a coupled eigenvalue problem is solved for the free part of the system. The expressions for the macroscopic effective quantities, i.e. macroscopic flux, rate of change of concentration field and the macroscopic stress, are finally obtained. As an emergent result of the model reduction at the microscale, a coupled diffusion–mechanics enriched continuum is obtained, in which the fully resolved microscopic coupled system of equations is replaced by a set of ordinary differential equations which are computationally inexpensive to solve. Numerical examples are presented, and a comparison is made between the fully resolved finite element calculations and the reduced order model for the cathode–electrolyte system of a lithium ion battery. The proposed reduced order homogenization has been shown to capture the coupled behavior with an excellent accuracy and largely improved computational efficiency.

Possible extensions to the current work are:

- two-scale implementation of the coupled diffusion–mechanics enriched continuum, which can be compared to direct numerical simulations;
- non-linear regimes, both for elasticity and mass diffusion, can be analyzed, for example, by using model reduction technique with modal derivatives in combinations with a discrete empirical interpolation for the non-linear forcing terms [43];
- inelastic regimes and large deformations can be performed by using appropriate model reduction methods, e.g. using proper generalized decomposition, at the microscale [44].

Abbreviations

DNS: Direct numerical simulations; RVE: Representative volume element; DOF: Degree of freedom; ODE: Ordinary differential equation; FE: Finite element; ROM: Reduced order method; CTH: Transient computational homogenization; RTH: Reduced computational homogenization.

Acknowledgements

Support for this research was provided by European Commission through an Erasmus Mundus grant in the framework of the Simulation in Engineering and Entrepreneurship Development (SEED) program.

Authors' contributions

All authors participated in the definition of the methods. AW implemented the methods, realized all computations. All authors contributed to the writing of the manuscript. All authors read and approved the final manuscript.

Funding

SEED program is an initiative of 8 universities Partners, managed by EACEA and financed by the European Commission with grant Ref. 2013-0043.

Competing interests
The authors declare that they have no competing interests.

Author details
[1]Institut de Recherche en Génie Civil et Mécanique, GeM, UMR 6183-CNRS-École Centrale de Nantes-Université de Nantes, 44321 Nantes, France, [2]Department of Mechanical Engineering, Eindhoven University of Technology, 5600 MB Eindhoven, The Netherlands.

Received: 3 November 2019 Accepted: 3 March 2020
Published online: 28 March 2020

References

1. Chu JL, Lee S. The effect of chemical stresses on diffusion. J Appl Phys. 1994;75(6):2823–9.
2. Yang F. Interaction between diffusion and chemical stresses. Mater Sci Eng A. 2005;409(1–2):153–9.
3. Marmarou A. A review of progress in understanding the pathophysiology and treatment of brain edema. Neurosurg Focus. 2007;22(5):1–10.
4. Gupta D, Ho PS. Diffusion phenomena in thin films and microelectronic materials. Park Ridge: Noyes Data Corporation; 1989. p. 588.
5. Cui Z, Gao F, Qu J. A finite deformation stress-dependent chemical potential and its applications to lithium ion batteries. J Mech Phys Solids. 2012;60(7):1280–95.
6. Aziz MJ. Thermodynamics of diffusion under pressure and stress: relation to point defect mechanisms. Appl Phys Lett. 1997;70(21):2810–2.
7. Eremeev VS, Mikhailov VN, Boiko EB. Analysis of the level of concentration stresses and their effect on the mass transport process under diffusion saturation. Mat Met Fiz-Mekh Polya. 1983;17:43–8.
8. Frohberg G. Diffusion and atomic transport. Materials sciences in space. Berlin: Springer; 1986. p. 93–128.
9. Gurtin ME, Fried E, Anand L. The mechanics and thermodynamics of continua. Cambridge: Cambridge University Press; 2010.
10. Herring C. Diffusional viscosity of a polycrystalline solid. J Appl Phys. 1950;21(5):437–45.
11. Zener C. Elasticity and anelasticity of metals. Chicago: University of Chicago press; 1948.
12. Aifantis EC. On the problem of diffusion in solids. Acta Mech. 1980;37(3–4):265–96.
13. Gorsky WS. Theorie der elastischen nachwirkung in ungeordneten mischkristallen (elastische nachwirkung zweiter art). Physikalische Zeitschrift der Sowjetunion. 1935;8:457–71.
14. Golmon S, Maute K, Dunn ML. Numerical modeling of electrochemical-mechanical interactions in lithium polymer batteries. Comput Struct. 2009;87(23–24):1567–79.
15. Swallow JG, Woodford WH, Chen Y, Lu Q, Kim JJ, Chen D, Chiang YM, Carter WC, Yildiz B, Tuller HL, Van Vliet KJ. Chemomechanics of ionically conductive ceramics for electrical energy conversion and storage. J Electroceram. 2014;32(1):3–27.
16. Zhang X, Shyy W, Sastry AM. Numerical simulation of intercalation-induced stress in Li-ion battery electrode particles. J Electrochem Soc. 2007;154(10):A910–6.
17. Grazioli D, Magri M, Salvadori A. Computational modeling of Li-ion batteries. Comput Mech. 2016;58(6):889–909.
18. Zhao K, Pharr M, Vlassak JJ, Suo Z. Fracture of electrodes in lithium-ion batteries caused by fast charging. J Appl Phys. 2010;108(7):073517.
19. Golmon S, Maute K, Dunn ML. Multiscale design optimization of lithium ion batteries using adjoint sensitivity analysis. Int J Numer Methods Eng. 2012;92(5):475–94.
20. Chiang YM, Hellweg B. Reticulated and controlled porosity battery structures, June 30 2009. US Patent 7,553,584.
21. Larché F, Cahn JW. A linear theory of thermochemical equilibrium of solids under stress. Acta Metall. 1973;21(8):1051–63.
22. Ko SC, Lee S, Chou YT. Chemical stresses in a square sandwich composite. Mater Sci Eng A. 2005;409(1–2):145–52.
23. Ebner M, Geldmacher F, Marone F, Stampanoni M, Wood V. X-ray tomography of porous, transition metal oxide based lithium ion battery electrodes. Adv Energy Mater. 2013;3(7):845–50.
24. Kaessmair S, Steinmann P. Computational first-order homogenization in chemo-mechanics. Arch Appl Mech. 2018;88(1–2):271–86.
25. Geers MGD, Kouznetsova VG, Brekelmans WAM. Multi-scale computational homogenization: trends and challenges. J Comput Appl Math. 2010;234(7):2175–82.
26. Miehe C, Koch A. Computational micro-to-macro transitions of discretized microstructures undergoing small strains. Arch Appl Mech. 2002;72(4–5):300–17.
27. Ender M, Joos J, Carraro T, Ivers-Tiffée E. Three-dimensional reconstruction of a composite cathode for lithium-ion cells. Electrochem Commun. 2011;13(2):166–8.
28. Brassart L, Stainier L. Effective transient behaviour of heterogeneous media in diffusion problems with a large contrast in the phase diffusivities. J Mech Phys Solids. 2019;124:366–91.
29. Salvadori A, Bosco E, Grazioli D. A computational homogenization approach for Li-ion battery cells: part 1-formulation. J Mech Phys Solids. 2014;65:114–37.
30. Salvadori A, Grazioli D, Geers MGD. Governing equations for a two-scale analysis of Li-ion battery cells. Int J Solids Struct. 2015;59:90–109.
31. Waseem A, Heuzé T, Stainier L, Geers MGD, Kouznetsova VG. Model reduction in computational homogenization for transient heat conduction. Comput Mech. 2020;65:249–66.
32. Sridhar A, Kouznetsova VG, Geers MGD. Homogenization of locally resonant acoustic metamaterials towards an emergent enriched continuum. Comput Mech. 2016;57(3):423–35.
33. Grazioli D. Multiscale and multiphysics modeling of li-ion battery cells. PhD thesis, Università degli Studi di Brescia; 2015.

34. Kaessmair S, Steinmann P. Comparative computational analysis of the Cahn–Hilliard equation with emphasis on c1-continuous methods. J Comput Phys. 2016;322:783–803.
35. Auriault JL, Boutin C, Geindreau C. Homogenization of coupled phenomena in heterogenous media, vol. 149. Hoboken: Wiley; 2010.
36. Larsson F, Runesson K, Su F. Variationally consistent computational homogenization of transient heat flow. Int J Numer Methods Eng. 2010;81(13):1659–86.
37. De Souza Neto EA, Blanco PJ, Sánchez PJ, Feijóo RA. An RVE-based multiscale theory of solids with micro-scale inertia and body force effects. Mech Mater. 2015;80:136–44.
38. Pham K, Kouznetsova VG, Geers MGD. Transient computational homogenization for heterogeneous materials under dynamic excitation. J Mech Phys Solids. 2013;61(11):2125–46.
39. Ramos GR, dos Santos T, Rossi R. An extension of the Hill-Mandel principle for transient heat conduction in heterogeneous media with heat generation incorporating finite RVE thermal inertia effects. Int J Numer Methods Eng. 2017;111(6):553–80.
40. Ji Liang, Guo Zhansheng. Analytical modeling and simulation of porous electrodes: li-ion distribution and diffusion-induced stress. Acta Mech Sin. 2018;34(1):187–98.
41. Sonon B, Francois B, Massart TJ. A unified level set based methodology for fast generation of complex microstructural multi-phase RVEs. Comput Methods Appl Mech Eng. 2012;223:103–22.
42. Wu B, Lu W. A battery model that fully couples mechanics and electrochemistry at both particle and electrode levels by incorporation of particle interaction. J Power Sour. 2017;360:360–72.
43. Weeger Oliver, Wever Utz, Simeon Bernd. Nonlinear frequency response analysis of structural vibrations. Comput Mech. 2014;54(6):1477–95.
44. Chinesta F, Cueto E. PGD-based modeling of materials. Structures and processes. Berlin: Springer; 2014.

Publisher's Note